DESY 18-025, FR-PHENO-2018-003, KA-TP-05-2018, ZU-TH-08/18 manuscript No.
(will be inserted by the editor)

Precise predictions for same-sign W-boson scattering at the LHC

Alessandro Ballestrero[1], Benedikt Biedermann[2], Simon Brass[3], Ansgar Denner[2], Stefan Dittmaier[4], Rikkert Frederix[5], Pietro Govoni[6], Michele Grossi[7,8], Barbara Jäger[9], Alexander Karlberg[10], Ezio Maina[1,11], Mathieu Pellen[2], Giovanni Pelliccioli[1,11], Simon Plätzer[12], Michael Rauch[13], Daniela Rebuzzi[7], Jürgen Reuter[14], Vincent Rothe[14], Christopher Schwan[4], Hua-Sheng Shao[15], Pascal Stienemeier[14], Giulia Zanderighi[16], Marco Zaro[17], Dieter Zeppenfeld[13]

[1] INFN, Sezione di Torino, Via P. Giuria 1, 10125 Turin, Italy
[2]Universität Würzburg, Institut für Theoretische Physik und Astrophysik, Emil-Hilb-Weg 22, 97074 Würzburg, Germany
[3]Universität Siegen, Department Physik, Walter-Flex-Str.3, 57068 Siegen, Germany
[4]Albert-Ludwigs-Universität Freiburg, Physikalisches Institut, Hermann-Herder-Str. 3, 79104 Freiburg, Germany
[5]Technische Universität München, James-Franck-Str. 1, 85748 Garching, Germany
[6]University and INFN, Milano-Bicocca, piazza della Scienza, 3, 2016 Milan, Italy
[7]Universitá di Pavia, Dipartimento di Fisica and INFN, Sezione di Pavia, Via A. Bassi 6, 27100 Pavia, Italy
[8]IBM Italia s.p.a. Circonvallazione Idroscalo, 20090 Segrate (MI), Italy
[9]University of Tübingen, Institute for Theoretical Physics, Auf der Morgenstelle 14, 72076 Tübingen, Germany
[10]Universität Zürich, Physik-Institut, Winterthurerstrasse 190, 8057 Zürich, Switzerland
[11]Università di Torino, Dipartimento di Fisica, Via P. Giuria 1, 10125 Turin, Italy
[12]University of Vienna, Particle Physics, Faculty of Physics, Vienna, Austria
[13]Karlsruhe Institute of Technology (KIT), Institute for Theoretical Physics, 76131 Karlsruhe, Germany
[14]DESY Theory Group, Notkestr. 85, 22607 Hamburg, Germany
[15]Sorbonne Université et CNRS, Laboratoire de Physique Théorique et Hautes Énergies (LPTHE), UMR 7589, 4 place Jussieu, 75252 Paris Cedex 05, France
[16]CERN, Theoretical Physics Department, 1211, Geneva 23, Switzerland
[17]Nikhef, Science Park 105, 1098XG Amsterdam, The Netherlands

the date of receipt and acceptance should be inserted later

Abstract

Vector-boson scattering processes are of great importance for the current run-II and future runs of the Large Hadron Collider. The presence of triple and quartic gauge couplings in the process gives access to the gauge sector of the Standard Model and possible new-physics contributions there. To test this hypothesis, sound knowledge of the Standard Model contributions is necessary, with a precision which at least matches the experimental uncertainties of existing and forthcoming measurements. In this article we present a detailed study of the vector-boson scattering process with two positively-charged leptons and missing transverse momentum in the final state, mediated predominantly by same-sign production of two W bosons with positive charge. In particular, we first carry out a systematic comparison of the various approximations that are usually performed for this kind of process against the complete calculation, at LO and NLO QCD accuracy. Such a study is performed both in the usual fiducial region used by experimental collaborations and in a more inclusive phase space, where the differences among the various approximations lead to more sizeable effects. Afterwards, we turn to predictions matched to parton showers, at LO and NLO: we show that on the one hand, the inclusion of NLO QCD corrections leads to more stable predictions, but on the other the details of the matching and of the parton-shower programs lead to differences which are considerably larger than those observed at fixed-order, even in the experimental fiducial region. We conclude with some recommendations for experimental studies of vector-boson scattering processes.

1 Introduction

Vector-boson scattering (VBS) at a hadron collider usually refers to the interaction of massive vector-bosons ($W^{\pm}, Z$), radiated by partons (quarks) of the incoming protons, which in turn are deflected from the beam direction and enter the volume of the particle detectors. As a consequence, the typical signature of VBS events is characterised by two energetic jets and four fermions, originating from the decay of the two vector bosons. Among the possible diagrams, the scattering process can be mediated by a Higgs boson and involves in particular its longitudinal component. The interaction of longitudinally polarised bosons is of particular interest, because the corresponding matrix elements feature unitarity cancellations that strongly depend on the actual structure of the Higgs sector. A detailed study of this class of processes will therefore further constrain the Higgs couplings at a very different energy scale with respect to the Higgs boson mass, and hint at, or exclude, non-Standard Model behaviours.

The VBS process involving two same-sign W bosons has the largest signal-to-background ratio at the LHC of all the VBS processes: evidence for it was found at the centre-of-mass energy of 8 TeV already [1, 2], and it has been recently observed [3] and measured [4] at 13 TeV as well. Presently, the measurements of VBS processes are limited by statistics, but the situation will change in the near future. On the theoretical side, it is thus of prime importance to provide predictions with systematic uncertainties at least comparable to the current and envisaged experimental precision [5].

W^+W^+ scattering is also the simplest VBS process to calculate, because the double-charge structure of the leptonic final state limits the number of partonic processes and total number of Feynman diagrams for each process. Nonetheless, it possesses all features of VBS at the LHC and is thus representative of other VBS signatures. Therefore, this process is the ideal candidate for a comparative study of the different simulation tools.

In the last few years, several next-to-leading order (NLO) computations have become available for both the VBS process [6–12] and its QCD-induced irreducible background process [12–16]. All these VBS computations rely on various approximations, typically neglecting contributions which are expected to be small under realistic experimental setups [11, 17]. Recently, the complete NLO corrections to W^+W^+ have been evaluated in Ref. [18], making it possible for the first time to study in detail the quality of the VBS approximations at NLO QCD.

After having defined the VBS process in Sec. 2 and having described the approximations of the various computer codes in Sec. 3, in Sec. 4 a leading-order (LO) study of the different contributions which lead to the production of two same-sign W bosons and two jets is performed, as a function of typical VBS cuts. In the same section predictions for VBS from different tools are compared at the level of the cross section and differential distributions. The article continues in Sec. 5 where the comparison is extended to the NLO corrections to VBS. The effect of the inclusion of matching LO and NLO computations to parton-shower (PS) is discussed in Sec. 6. Finally, Sec. 7 contains a summary of the article and concluding remarks.

Preliminary results of the present study have already been made public in Ref. [19].

2 Definition of the process

The scattering of two positively-charged W bosons with their subsequent decay into different-flavour leptons can proceed at the LHC through the partonic process:

$$\mathrm{pp} \to \mu^+\nu_\mu \mathrm{e}^+\nu_\mathrm{e}\,\mathrm{jj} + \mathrm{X}. \tag{1}$$

This process possesses three LO contributions of different orders. At LO, this process can proceed via three different coupling-order combinations: $\mathcal{O}(\alpha^6)$, $\mathcal{O}(\alpha_\mathrm{s}2\alpha^4)$, and $\mathcal{O}(\alpha_\mathrm{s}\alpha^5)$. The first, commonly referred to as EW contribution or VBS [1], receives the contributions from Feynman diagrams such as those in Fig. 1: in addition to genuine VBS contributions (left diagram), it also features s-channel contributions with non-resonant vector bosons (center diagram) or from triple-boson production (right diagram). Note that s-, t-, and u-channel contributions are defined according to the quark lines. s-channel denotes all Feynman diagrams where the two initial-state partons are connected by a continuous fermion line. u-channel refers to contributions with crossed fermion lines, which appears for identical quarks or anti-quarks in the final state The s-channel contributions will play a particular role in the study of the various contributions in Sec. 4.1.

When using approximations, care must be taken that only gauge-invariant subsets are considered to obtain physically meaningful results. We will discuss the commonly-used possible choices in detail in the next section.

The second coupling combination corresponds to diagrams with a gluon connecting the two quark lines, and with the W bosons radiated off the quark lines. Because of the different colour structure, this contribution features a different kinematical behaviour than

[1] The name VBS is used even though not all Feynman diagrams involve the scattering of vector bosons.

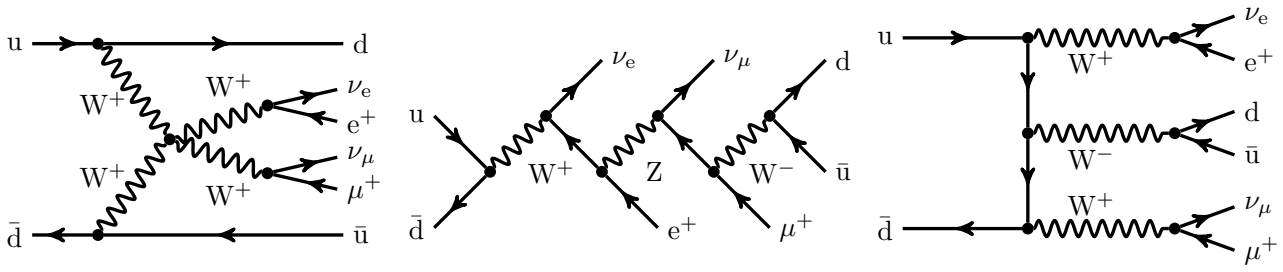

Fig. 1: Sample tree-level diagrams that contribute to the process $pp \to \mu^+\nu_\mu e^+\nu_e jj$ at order $\mathcal{O}(\alpha^6)$. In addition to typical VBS contributions (left), this order also possesses s-channel contributions such as decay chain (middle) and tri-boson contributions (right).

VBS. Nonetheless they share the same final state, and this class of contributions therefore constitutes an irreducible background to the genuine VBS signal.

Finally, the third contribution is the interference of the two types of amplitudes described above. It is non-zero only for those partonic subprocesses which involve only one quark family. Such a contribution is typically small but not negligible for realistic experimental setups [18].

In experimental measurements, special cuts, called VBS cuts, are designed to enhance the EW contribution over the QCD one and to suppress the interference. These cuts are based on the different kinematical behaviour of the two contributions. The EW contribution is characterised by two jets with large rapidities as well as a large invariant mass. The two W bosons are mostly produced centrally. This is in contrast to the QCD contribution which favours jets in the central region. Therefore, the event selection usually involves rapidity-difference and invariant-mass cuts for the jets. Note that, as pointed out in Ref. [18], when considering full amplitudes, the separation between EW and QCD production becomes ill defined. Hence, combined measurements which are better theoretically defined should be preferably performed by the experimental collaborations at the LHC.

3 Details of the calculations

3.1 Several descriptions for one process

We now turn to discuss the various approximations which are implemented in computer programs for the EW contribution at $\mathcal{O}(\alpha^6)$. Since we are mostly interested in the scattering of two W gauge bosons, which includes the quartic gauge-boson vertex, may appear justified to approximate the full process by considering just those diagrams which contain the $2 \to 2$ scattering process as a sub-part. However, this set of contributions is not gauge invariant. In order ensure gauge invariance, an on-shell projection of the incoming and outgoing W bosons should be performed **MZ CITE**. Unfortunately, the former momenta are space-like and thus a simple on-shell projection is not possible. Instead, one can keep the W boson legs connected to the external quark line off-shell while the ones connected to the final-state leptons, which are already time-like, are put on-shell. [MZ: is this still gauge invariant? if so, one should change the sentence above "In order to ensure.."] Then the polarisation of the gauge boson is accommodated following for example the implementations of Refs. [20, 21]. Such an approximation is usually called effective vector-boson approximation (EVBA) [22–24].

An improvement of such an approximation consists in considering all t- and u-channel diagrams and squaring them separately, neglecting interference contributions between the two classes. These interferences are expected to be small in the VBS fiducial region, as they are both phase-space and colour suppressed [17, 11]. The s-channel squared diagrams and any interferences between them and the t/u-channels are also discarded. This approximation is often called t-/u- approximation, VBF, or even VBS approximation. We will adopt the latter denomination in the following of the article. This approximation is gauge-invariant, a fact that can be appreciated by considering the two incoming quarks as belonging to two different copies of the SU(3) gauge group.

A further refinement is to add to the VBS approximation the squared matrix element of the s-channel contributions.

The approximations performed at LO can be extended when NLO QCD corrections to the order $\mathcal{O}(\alpha^6)$ are computed. The VBS approximation can be extended at NLO in a straightforward manner for what concerns the virtual contributions. For the real-emission

contributions special care must be taken for the gluon-initiated processes[2].

A further refinement is to consider the full real contributions, which include all interferences, and part of the virtual. In particular one can consider only one-loop amplitudes where there is no gluon exchange between the two quark lines and assuming a cancellation of the infrared (IR) poles.

When considering the full one-loop amplitude of order $\mathcal{O}(g_s^2 g^6)$ squared with the tree amplitude of order $\mathcal{O}(g^6)$, not only real QCD radiation but also QED ones have to be included in order cancel IR singularities. But all IR singularities related to photon emissions are not cancelled by the above mentioned virtual corrections. Another type of virtual corrections has to be incorporated, namely the one-loop amplitude of order $\mathcal{O}(g^8)$ interfered with the tree-level one of order $\mathcal{O}(g_s^2 g^4)$. Hence the full NLO corrections of order $\mathcal{O}\left(\alpha_s \alpha^6\right)$ consist not only of QCD-type corrections but also of EW ones [18].

3.2 Description of the predictions

In the following, the codes employed throughout this paper and the approximations implemented in each of them will be discussed:

- The program Bonsay consists of a general-purpose Monte Carlo integrator written by Christopher Schwan and matrix elements taken from different sources: Born matrix elements are adapted from the program Lusifer [25], real matrix elements are written by Marina Billoni, and virtual matrix elements by Stefan Dittmaier. One loop integrals are evaluated using the Collier library [26, 27]. For the fiducial cross sections it uses the VBS approximation at LO and NLO. The virtuals are additionally approximated using a double pole approximation. For more inclusive cross sections at LO the exact matrix elements (s-channels, interferences) are used.
- MadGraph5_aMC@NLO [28] is an automatic meta-code (a code that generates codes) which makes it possible to simulate any scattering process including NLO QCD corrections both at fixed order and including matching to parton showers. It makes use of the FKS subtraction method [29, 30] (automated in the module MadFKS [31, 32]) for regulating IR singularities. The computations of one-loop amplitudes are carried out by switching dynamically between two integral-reduction techniques, OPP [33] or Laurent-series expansion [34], and TIR [35–37]. These have been automated in the module MadLoop [38], which in turn exploits CutTools [39], Ninja [40, 41], IREGI [42], or Collier [27], together with an in-house implementation of the OpenLoops optimisation [43]. Finally, scale and PDF uncertainties can be obtained in an exact manner via reweigthing at zero additional CPU cost [44].
  The simulation of VBS at NLO-QCD accuracy can be performed by issuing the following commands in the program interface:

```
> set complex_mass_scheme
> import model loop_qcd_qed_sm_Gmu
> generate p p > e+ ve mu+ vm j j QCD=0 [QCD]
> output
```

  With these commands the complex-mass scheme is turned on, then the NLO-capable model is loaded[3], finally the process code is generated (note the `QCD=0` syntax to select the purely-electroweak process) and written to disk. No approximation is performed for the Born and real-emission matrix elements. For what concerns the virtual matrix element, because of some internal limitations which will be lifted in the future version capable of computing both QCD and EW corrections, only loops with QCD-interacting particles are generated. Such an approximation is equivalent to the assumption that the finite part of those loops which feature EW bosons is zero. In practice, since a part of the contribution to the single pole is also missing, the internal pole-cancelation check at run time has to be turned off, by setting the value of the `IRPoleCheckThreshold` and `PrecisionVirtualAtRunTime` parameters in the `Cards/FKS_params.dat` file to -1.
- The program MoCaNLO+Recola is made of a flexible Monte Carlo program dubbed MoCaNLO and of the matrix element generator Recola [45, 46]. It can compute arbitrary processes for the LHC at both NLO QCD and EW accuracy in the Standard Model. This is made possible by the fact that Recola can compute arbitrary processes at tree and one-loop level in the Standard Model. To that end, it relies on the Collier library [26, 27] to numerically evaluate the one-loop scalar and tensor integrals. In addition, the subtraction of the IR divergences appearing in the real corrections has been au-

[2] The initial-state gluon and quark must not couple together, otherwise infrared divergences proportional to s-channels will appear, which do not match with the ones found in the virtual contributions. The subset of diagrams where all couplings of the initial state gluon to initial state quark are neglected forms a gauge-invariant subset, with the same argument presented above.

[3] Despite the `loop_qcd_qed_sm_Gmu` model also includes NLO counterterms for computing electro-weak corrections, it is not yet possible to compute such corrections with the current version of the code.

Code	$\mathcal{O}(\alpha^6)$ $\lvert s\rvert^2/\ \lvert t\rvert^2/\lvert u\rvert^2$	$\mathcal{O}(\alpha^6)$ interf.	Non-res.	NLO	NF QCD	EW corr. to $\mathcal{O}(\alpha_s\alpha^5)$
Bonsay	t/u	No	Yes, virt. No	Yes	No	No
Powheg	t/u	No	Yes	Yes	No	No
MG5_aMC	Yes	Yes	Yes	Yes	No virt.	No
MoCaNLO+Recola	Yes	Yes	Yes	Yes	Yes	Yes
PHANTOM	Yes	Yes	Yes	No	-	-
VBFNLO	Yes	No	Yes	Yes	No	No
Whizard	Yes	Yes	Yes	No	-	-

Table 1: Summary of the different properties of the codes employed in the comparison.

tomatised thanks to the Catani–Seymour dipole formalism for both QCD and QED [47, 48]. The code has demonstrated its ability to compute at NLO high multiplicity processes up to $2 \to 7$ [49, 50]. In particular the full NLO corrections to VBS and its irreducible background [51, 18] have been obtained from this tool. One key aspect for these high multiplicity processes is the fast integration which is ensured by using similar phase-space mappings to those of Refs. [52, 53, 25]. In MoCaNLO+Recola no approximation is performed at LO as well as at NLO, and, in particular, also contributions stemming from EW corrections to the interference are computed.

– Phantom [54] is a dedicated tree-level Monte Carlo for six parton final states at pp, $p\bar{p}$ and e^+e^- colliders at orders α^6 and $\alpha_s^2\alpha^4$ including interferences between the two sets of diagrams. It employs complete tree-level matrix elements in the complex-mass scheme [53, 55, 56] computed via the modular helicity formalism [57, 58]. The integration uses a multi-channel approach [59] and an adaptive strategy [60]. Phantom generates unweighted events at parton level for both the SM and a few instances of BSM theories.
– The Powheg-Box [61–63] is a framework for matching NLO-QCD calculations with parton showers. It relies on the user providing the matrix elements and Born phase space, but will automatically construct FKS [29] subtraction terms and the phase space for the real emission. For the VBS processes all matrix elements are being provided by a previous version of VBFNLO [64, 65, 16] and hence the approximations used in the Powheg-Box are the similar to those used in VBFNLO.
– VBFNLO [64, 65, 16] is a flexible parton-level Monte Carlo for processes with electroweak bosons. It allows the calculation of VBS processes at NLO QCD in the VBS approximation, with process IDs between 200 and 290. The corresponding s-channel contributions are available separately as triboson processes with semi-leptonic decays, with process IDs in the 400 range. These can simply be added on top of the VBS contribution, as interferences between the two are neglected. The usage of leptonic tensors in the calculation, pioneered in Ref. [6], thereby leads to a significant speed improvement over automatically generated code. Besides the SM, also a variety of new-physics models including anomalous couplings of the Higgs and gauge bosons can be simulated.
– Whizard [66, 67] is a multi-purpose event generator with the LO matrix element generator O'Mega. [MZ: if NLO results for this processes cannot be provided, we should skip what follows, or at least clarify the limitations] provides FKS subtraction terms for any NLO process, while virtual matrix elements are provided externally by OpenLoops [43] (alternatively, Recola [45, 46] (cf. above) can be used as well). Whizard allows to simulate a huge number of BSM models as well, in particular for new physics in the VBS channel in terms of both higher-dimensional operators as well as explicit resonances.

We conclude this section by summarizing the details of the various codes in Tab. 1. In particular, it is specified whether

– all s- and t/u-channel diagrams that lead to the considered final state are included;
– interferences between diagrams are included at LO;
– diagrams which do not feature two resonant vector bosons are included;
– the so-called non-factorisable (NF) QCD corrections, *i.e.* the corrections where (real or virtual) gluons are exchanged between different quark lines, are included;
– EW corrections to the $\mathcal{O}(\alpha^5\alpha_s)$ interference are included. These corrections are of the same order as the NLO QCD corrections to the $\mathcal{O}(\alpha^6)$ term.

3.3 Input parameters

The hadronic scattering processes are simulated at the LHC with a center-of-mass energy $\sqrt{s} = 13\,\text{TeV}$. The

NNPDF 3.0 parton distribution functions (PDFs) [68] with five massles flavour,[4] NLO-QCD evolution, and a strong coupling constant $\alpha_s(M_Z) = 0.118$ are employed.[5][6] Initial-state collinear singularities are factorised according to the $\overline{\text{MS}}$ scheme, consistently with what is done in NNPDF.

For the massive particles, the following masses and decay widths are used:

$$\begin{aligned} m_t &= 173.21\,\text{GeV}, & \Gamma_t &= 0\,\text{GeV}, \\ M_Z^{\text{OS}} &= 91.1876\,\text{GeV}, & \Gamma_Z^{\text{OS}} &= 2.4952\,\text{GeV}, \\ M_W^{\text{OS}} &= 80.385\,\text{GeV}, & \Gamma_W^{\text{OS}} &= 2.085\,\text{GeV}, \\ M_H &= 125.0\,\text{GeV}, & \Gamma_H &= 4.07\times10^{-3}\,\text{GeV}. \end{aligned} \tag{2}$$

The measured on-shell (OS) values for the masses and widths of the W and Z bosons are converted into pole values for the gauge bosons ($V = \text{W}, \text{Z}$) according to Ref. [70],

$$\begin{aligned} M_V &= M_V^{\text{OS}}/\sqrt{1+(\Gamma_V^{\text{OS}}/M_V^{\text{OS}})^2}\,, \\ \Gamma_V &= \Gamma_V^{\text{OS}}/\sqrt{1+(\Gamma_V^{\text{OS}}/M_V^{\text{OS}})^2}. \end{aligned} \tag{3}$$

The EW coupling is renormalised in the G_μ scheme [71], where

$$G_\mu = 1.16637\times10^{-5}\,\text{GeV}^{-2}. \tag{4}$$

The numerical value of α, corresponding to the choice of input parameters is

$$1/\alpha = 132.3572\ldots\,. \tag{5}$$

The CKM-Matrix is assumed to be diagonal, meaning that the mixing between different quark families is neglected. The complex-mass scheme [53, 55, 56] is used throughout to treat unstable intermediate particles in a gauge-invariant manner.

The renormalisation and factorisation scales are set to the dynamical scale

$$\mu_{\text{ren}} = \mu_{\text{fac}} = \sqrt{p_{\text{T,j}_1}\,p_{\text{T,j}_2}}, \tag{6}$$

defined via the transverse momenta of the two hardest identified jets.[7] This choice of scale has been shown to provide stable NLO-QCD predictions [11].

Following experimental measurements [1, 4, 2, 72], the event selection used in the present study is:

– The two same-sign charged leptons are required to fulfill cuts on transverse momentum, rapidity, and separation in the rapidity-azimuthal angle separation,

$$p_{\text{T},\ell} > 20\,\text{GeV}, \qquad |y_\ell| < 2.5, \qquad \Delta R_{\ell\ell} > 0.3\,. \tag{7}$$

– The total missing transverse energy, computed from the vectorial sum of the transverse momenta of the two neutrinos, is required to be

$$E_{\text{T,miss}} = p_{\text{T,miss}} > 40\,\text{GeV}\,. \tag{8}$$

– QCD partons (light quarks and gluons) are clustered together using the anti-k_T algorithm [73] with distance parameter $R = 0.4$. We impose cuts on the jets' transverse momenta, rapidities, and their separation from leptons,

$$p_{\text{T,j}} > 30\,\text{GeV}, \qquad |y_\text{j}| < 4.5, \qquad \Delta R_{\text{j}\ell} > 0.3\,. \tag{9}$$

VBS cuts are applied on the two jets with largest transverse-momentum, unless otherwise stated. In particular, we impose a cut on the invariant mass of the di-jet system, as well as on the rapidity-separation of the two jets,

$$m_{\text{jj}} > 500\,\text{GeV}, \qquad |\Delta y_{\text{jj}}| > 2.5, \tag{10}$$

if not explicitly stated otherwise.

– When EW corrections are computed, real photons and charged fermions are clustered together using the anti-k_T algorithm with radius parameter $R = 0.1$. In this case, leptons and quarks are understood as *dressed fermions*.

4 Leading-order study

4.1 Three contributions

In the present section, the cross sections and distributions are obtained without applying the VBS cuts on m_{jj} and $|\Delta y_{\text{jj}}|$. In Tab. 2, the cross sections of the three contributions are reported. The EW, QCD, and interference contributions amount to 57%, 37%, and 6% of the total inclusive cross section, respectively. The QCD contribution does not posses external gluons due to charge conservation. Thus the $\mathcal{O}(\alpha_s^2\alpha^4)$ diagrams only involve gluon exchange in the t/u-channel between the quark lines. This results in a small contribution although the VBS cuts have not been imposed. The interference between EW and QCD contributions is small, due to color suppression, but not negligible (t/u interference with identical fermions).

In Fig. 2 these three contributions are shown separately and summed in the differential distribution of

[4] For the process considered, no bottom (anti-)quarks appear in the initial or final state at LO and NLO.

[5] The corresponding identifier `lhaid` in LHAPDF6 [69] is 260000.

[6] Note that the POWHEG-BOX uses its own implementation of the two loop running for α_s.

[7] The renormalisation and factorisation scale employed in the POWHEG-BOX slightly differ from the one defined in Eq. (6), as the momenta of two final-state quarks in the underlying-Born event are i employed instead of those of the two hardest jets.

Order	$\mathcal{O}(\alpha^6)$	$\mathcal{O}(\alpha_s^2\alpha^4)$	$\mathcal{O}(\alpha_s\alpha^5)$
σ[fb]	2.292 ± 0.002	1.477 ± 0.001	0.223 ± 0.003

Table 2: Cross sections at LO accuracy for the three contributions to the process pp $\to \mu^+\nu_\mu e^+\nu_e jj$, obtained with full matrix elements. These results are for the set-up described in Sec. 3.3, dropping the m_{jj} and $|\Delta y_{jj}|$ cuts.

the di-jet invariant mass m_{jj} and the rapidity difference $|\Delta y_{jj}|$. In the distributions in the di-jet invariant mass (left), one can observe that the EW contribution peaks around an invariant mass of about 80 GeV. These are due to diagrams where the two jets originate from the decay of a W boson (see middle and right diagrams in Fig. 1). Note that these contributions are not present in calculations relying on the VBS approximation. The EW contribution becomes dominant for di-jet invariant mass larger than 500 GeV. The same holds true for jet rapidity difference larger than 2.5 (right). This clearly explains why these two observables are used to enhanced the EW contribution over the QCD one. In particular, in order to have a large EW contribution, rather exclusive cuts are required.

This can also be seen in Fig. 3 where the three contributions are displayed as a function of the di-jet invariant mass and jet rapidity difference. Again, it is obvious that the region with low di-jet invariant mass should be avoided as it is dominated by tri-boson contributions. This motivates in particular the choice of $m_{jj} > 200$ GeV for our LO inclusive study (see below). Finally, let us notice that the choice $m_{jj} > 500$ GeV and $|\Delta y_{jj}| > 2.5$ made by the experimental collaborations is well motivated in order to enhance the EW contribution over its irreducible backgrounds. These are the cuts used in Sec. 4.3.

4.2 Inclusive comparison

In Fig. 4, ratios of double-differential cross sections in the plane $(m_{jj}, \Delta y_{jj})$ is shown. Two plots are displayed: the ratios of the $|t|^2+|u|^2$ and $|s|^2+|t|^2+|u|^2$ approximations over the full calculation. In the first case, the approximation is good within $\pm 10\%$ over the whole range apart in the low invariant-mass region at both low and large rapidity difference. The low rapidity difference region possesses remnants of the tri-bosons contributions that peak at di-jet invariant mass around the W-boson mass. It is therefore expected that the $|t|^2+|u|^2$ approximation fails in this region. The second plot, where the $|s|^2 + |t|^2 + |u|^2$ approximation is considered, displays a better behaviour in the previously mentioned region. The full calculation is approximated at the level of $\pm 5\%$ apart in the region where $\Delta y_{jj} < 2$. [AK: What are the MC error on these plots?]

Therefore, the *inclusive* study at NLO is only performed in the region

$$m_{jj} > 200\,\text{GeV} \qquad \text{and} \qquad |\Delta y_{jj}| > 2. \tag{11}$$

Hence, the differences arising at NLO in this fiducial region originate solely from NLO effects.

4.3 Comparison in the fiducial region

In Tab. 3, we report the total rates at LO accuracy obtained with the set-up described in Eqs. (7-9) with the VBS cuts $m_{jj} > 500$ GeV and $|\Delta y_{jj}| > 2.5$ (see Eq. (10)). The order considered here is the order $\mathcal{O}(\alpha^6)$. We note that several full predictions are not in statistical agreement. These are possibly due to Monte-Carlo integrators performing too aggressive estimations of statistical uncertainties. Nonetheless, all these predictions agree within less than 0.5%. At the level of the cross section, it seems difficult to infer the quality of the the various approximations. This simply means that the details of the various VBS approximations have an impact not larger than 0.5% at the level of the fiducial cross section at LO for a typical phase-space volume used by experimental collaborations. This is in agreement with the findings of Ref. [11, 17].

Code	σ[fb]
Bonsay	1.43636 ± 0.00002
MG5_aMC	1.4304 ± 0.0007
MoCaNLO+Recola	1.43476 ± 0.00009
PHANTOM	1.4374 ± 0.0006
Powheg-Box	1.44092 ± 0.00009
VBFNLO	1.43796 ± 0.00005
Whizard	1.4381 ± 0.0002

Table 3: Cross sections for the LHC process pp $\to \mu^+\nu_\mu e^+\nu_e jj$ at LO accuracy and order $\mathcal{O}(\alpha^6)$. The uncertainties shown refer to the estimated statistical error of the Monte Carlo programs. The predictions are obtained in the fiducial region described in Sec. 3.3.

In Fig. 5, we show the distributions in the invariant mass (left) and the rapidity difference of the two tagging jets (right) which are key observables for VBS measurements. In both cases we show the absolute distributions in the upper plot, while the lower plot displays the ratio over the predictions of MoCaNLO+Recola. For both observables we find a relatively good agreement among the various tools, which confirms the fact that

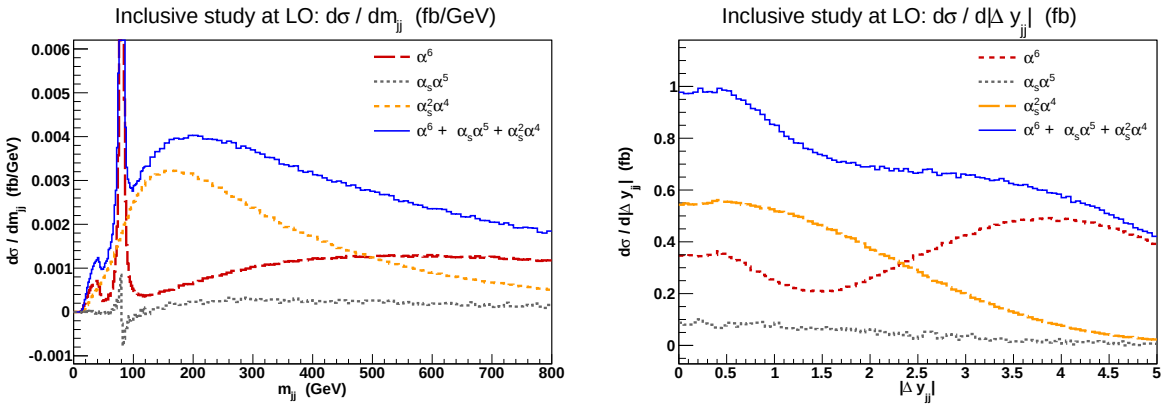

Fig. 2: Differential distribution in the di-jet invariant mass $m_{\rm jj}$ (left) and the difference of the jet rapidities $|\Delta y_{\rm jj}|$ (right) at LO. The EW contribution is in red, the QCD one in green, and the interference in grey. The sum of all the contributions is in blue. The cuts applied are the ones of of Sec. 3.3 but no cuts on $m_{\rm jj}$ and $|\Delta y_{\rm jj}|$ are applied.

contributions from s-channel diagrams as well as from non-resonant configurations are suppressed in the fiducial region. In general, the agreement is at the level of 1% or below for each bin. We have checked that the same level of agreement holds for other standard differential distributions such as rapidity, invariant mass, or transverse momentum. This means that at LO, in the fiducial volume and for energies relevant to the LHC, the VBS approximation is good to a per cent. This is in agreement with the findings of Sec. 4.2 as the present comparison completely excludes the phase-space region where tri-boson contributions could have a noticeable impact.

5 Next-to-leading order QCD

5.1 Inclusive comparision

We now present an inclusive study performed at NLO QCD for the EW component, namely the order $\mathcal{O}(\alpha_{\rm s}\alpha^6)$.

According to the results shown in Sec. 4.2, the VBS approximation at LO fails in the region $m_{\rm jj} < 200$ GeV, $|\Delta y_{\rm jj}| < 2$. For the inclusive region (see Eq. (11)), this approximation is good up to $\pm 10\%$ apart for large di-jet differences and low di-jet invariant mass. It is therefore interesting to check how good this approximation performs at NLO. Thus, we impose the same kinematic cuts shown in Sec. 3.3 and apply the VBS cuts of Eq. (11).

We compare three different predictions at NLO QCD: the VBS approximation ($|t|^2 + |u|^2$) implemented in Bonsay, the VBS approximation with the s-channel contributions ($|s|^2 + |t|^2 + |u|^2$) from VBFNLO, and the full computation. The full computation employs full matrix elements meaning that $t/u/s$ interferences, factorisable, and non-factorisable QCD corrections as well as EW corrections to the order $\mathcal{O}(\alpha_{\rm s}\alpha^6)$ are included. The total cross sections within the above mentioned kinematic cuts are shown in Tab. 4.

Prediction	$\sigma_{\rm tot}$ [fb]	δ[%]
full	1.8120 ± 0.0144	-
$\lvert t\rvert^2 + \lvert u\rvert^2$	1.6292 ± 0.0001	-10
$\lvert s\rvert^2 + \lvert t\rvert^2 + \lvert u\rvert^2$	1.7780 ± 0.0001	-2

Table 4: Total cross sections at NLO QCD *i.e.* at order $\mathcal{O}(\alpha_{\rm s}\alpha^6)$ for the full computation and two approximations. In addition to the cuts of Sec. 3.3, the VBS cuts take the values: $m_{\rm jj} > 200\,\text{GeV}$ and $|\Delta y_{\rm jj}| > 2$.

The VBS approximation for NLO QCD predictions (labelled by $|t|^2 + |u|^2$) is lower by about 10% with respect to the full calculation. The inclusion of s-channel diagrams improves the approximate prediction down to a 2%-level.

These differences are much more evident in differential distributions. In Fig. 6, we show the distributions in the di-jet invariant mass $m_{\rm jj}$ and rapidity separation $|\Delta y_{\rm jj}|$. For large $m_{\rm jj}$ and large $|\Delta y_{\rm jj}|$, as expected, the VBS approximation is performing well and its s-channel extension agree with the full calculation within 10% per cent. This is in contrast with the region $200\,\text{GeV} < m_{\rm jj} < 500\,\text{GeV}$ and $2 < |\Delta y_{\rm jj}| < 2.5$, the discrepancy between the $|t|^2 + |u|^2$ approximation and the full computation goes up to 30%. The inclusion of s-channels cures partly the discrepancy in this region. Still, for the very low $m_{\rm jj}$ a difference of about 5% remains [MP: To be checked the exact numerical value in data] . This might indicate that interference contri-

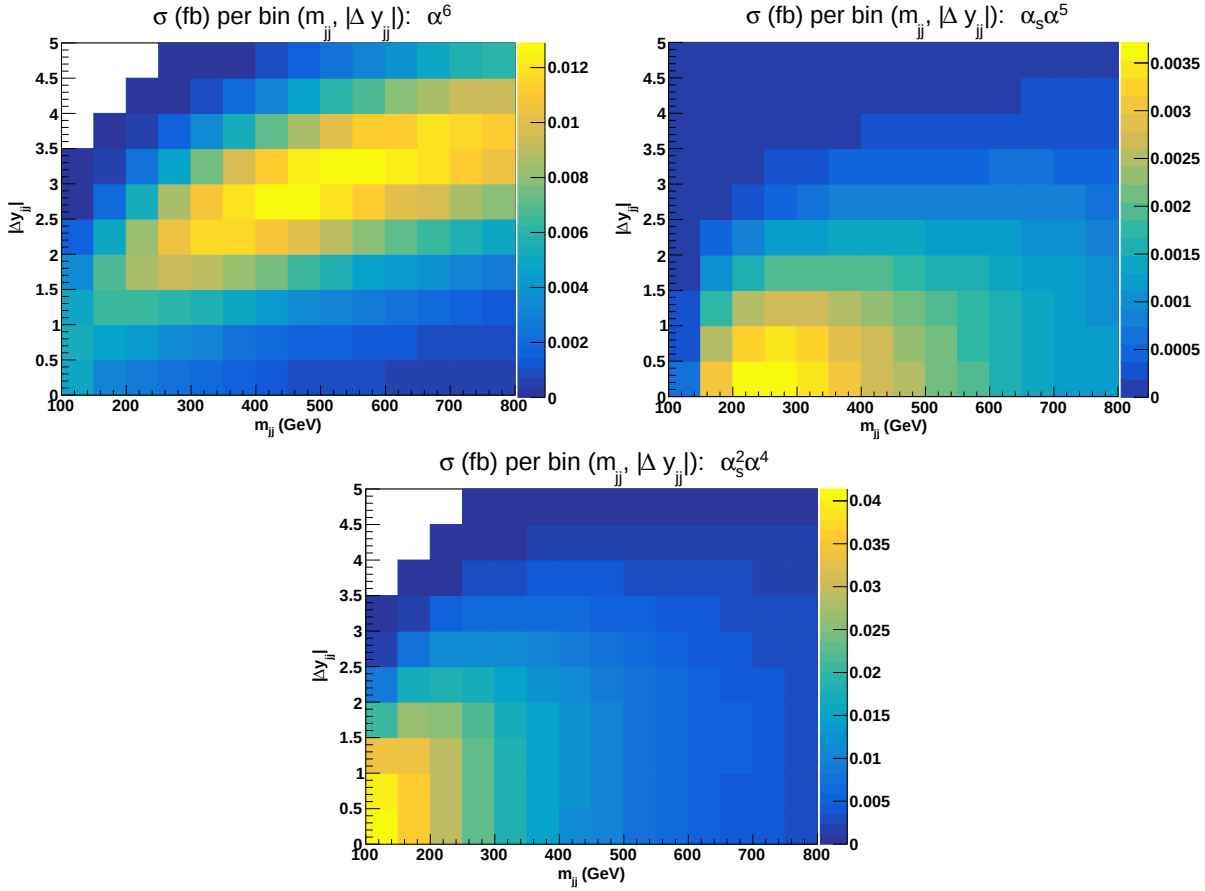

Fig. 3: Cross sections (fb) per bin in the plan $(m_{\rm jj}, \Delta y_{\rm jj})$ for the three LO contributions of orders $\mathcal{O}(\alpha^6)$ (top), $\mathcal{O}(\alpha_{\rm s}\alpha^5)$ (middle), and $\mathcal{O}(\alpha_{\rm s}^2\alpha^4)$ (bottom). The cuts applied are the ones of of Sec. 3.3 but no cuts on $m_{\rm jj}$ and $|\Delta y_{\rm jj}|$ are applied.

butions and/or non-factorisable QCD corrections play a non-negligible role in this phase-space region.

In order to investigate further the jet-pair kinematics, we look at the double-differential distribution in the variables $m_{\rm jj}$ and $\Delta y_{\rm jj}$. In particular, we compute in each bin the ratio of the approximated cross sections over the full one. In Fig. 7 we show the ratio $\sigma(|t|^2 + |u|^2)/\sigma(\text{full})$ and $\sigma(|s|^2 + |t|^2 + |u|^2)/\sigma(\text{full})$, in the left and right plot respectively.

As expected, in the low invariant mass–low rapidity separation region of the jet pair the VBS approximation fails significantly (up to 40% discrepancies). The inclusion of the s-channel brings the difference down to at most 5% [MP: To be checked the exact numerical value in data] . However, the positive discrepancy shown in the low $m_{\rm jj}$ region (black curve on the upper plots of Fig. 6) can be traced back to the low $m_{\rm jj}$, large $\Delta y_{\rm jj}$ region of Fig. 7.

The same positive discrepancy for the $|s|^2 + |t|^2 + |u|^2$ approximation, can be seen in the low transverse-momentum region of the leading jet in the upper plot of Fig. 8. In the large invariant mass–small rapidity separation region of Fig. 7, discrepancies at the level of 15% are present. This can be traced back to the large $p_{\rm T}$ and central rapidity region of the leading jets kinematics, shown in Fig. 8. For such distributions, despite the s-channel inclusion, the discrepancy between the approximated and full result is about $5-10\%$. In the VBS signal-region the VBS approximation shows a good agreement with the full calculation as documented in details below.

Concerning leptonic observables, we show in Fig. 9 the distributions of the lepton-lepton invariant mass and of the Zeppenfeld variable of the electron, defined as

$$z_{\rm e^+} = \frac{y_{\rm e^+} - \frac{y_{\rm j_1}+y_{\rm j2}}{2}}{|\Delta y_{jj}|}\,. \tag{12}$$

Analogous definitions will later also be used for the Zeppenfeld variable of the muon and of the third jet. The VBFNLO result for the $e^+\mu^+$ invariant mass agrees rather well with the full curve, obtained from MoCa-

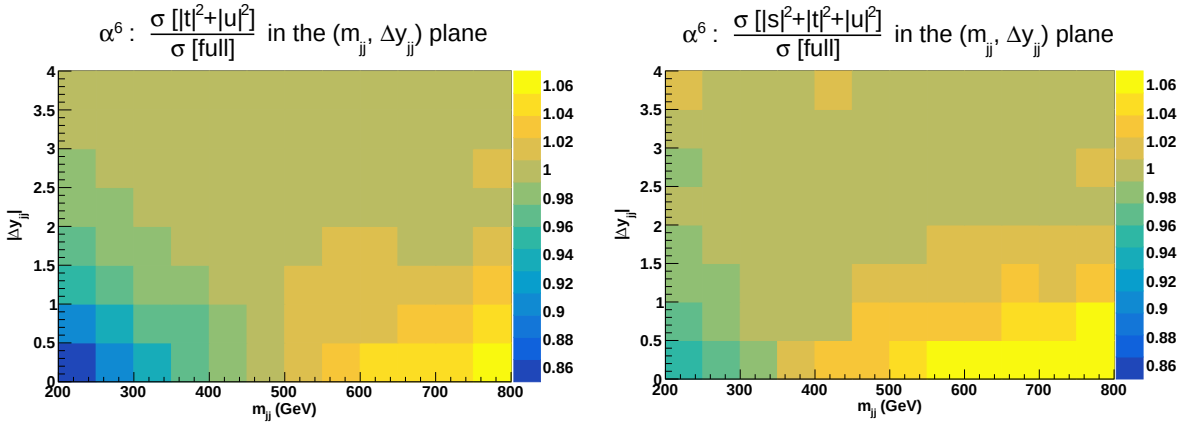

Fig. 4: Ratio of cross sections per bin in the plan $(m_{\rm jj}, |\Delta y_{\rm jj}|)$ at LO *i.e.* order $\mathcal{O}(\alpha^6)$. Ratio of approximated squared amplitudes over the full matrix element. The approximated squared amplitudes are computed as $|\mathcal{A}|^2 \sim |t|^2 + |u|^2$ (left) and $|\mathcal{A}|^2 \sim |s|^2 + |t|^2 + |u|^2$ (right). The cuts applied are the one of of Sec. 3.3 and no cuts on $m_{\rm jj}$ and $|\Delta y_{\rm jj}|$ are applied.

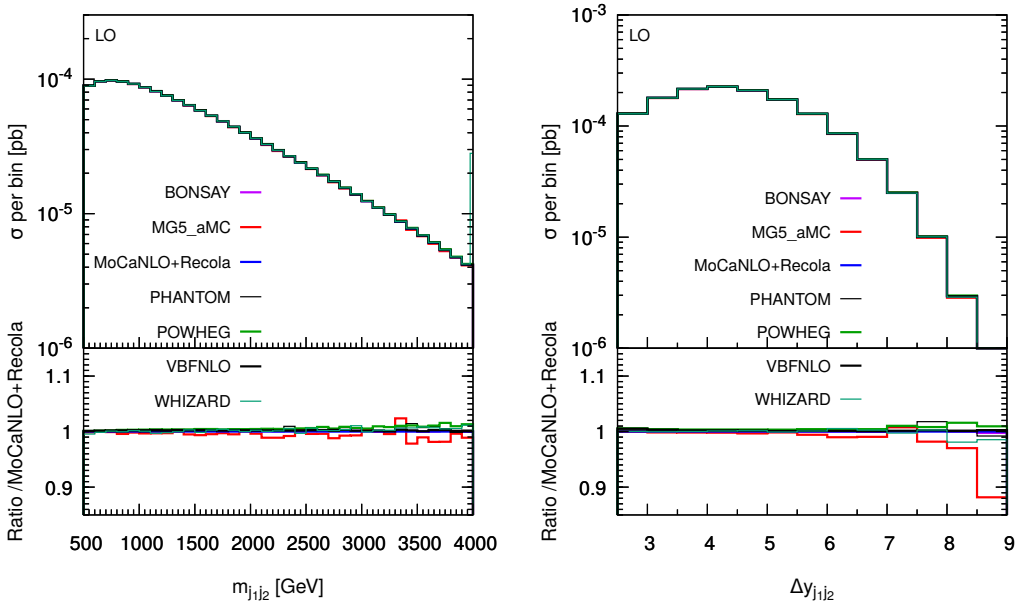

Fig. 5: Differential distributions in the invariant mass (left) and rapidity difference of the two tagging jets (right). The LHC process considered is pp $\to \mu^+\nu_\mu {\rm e}^+\nu_{\rm e}$jj at LO accuracy and order $\mathcal{O}(\alpha^6)$. The description of the different programs used can be found in Sec. 3.2. The upper plots provides the absolute value for each prediction while the lower plots presents all predictions normalised to MoCaNLO+Recola which is one of the full predictions. The predictions are obtained in the fiducial region described in Sec. 3.3.

NLO+Recola. The prediction from Bonsay is about 10% lower. The discrepancies are roughly constant over the whole spectrum. Instead, the right panel of Fig. 9 clearly shows that the Zeppenfeld variable of the positron z_e is strongly affected by the exclusion of s-channels, with increasing discrepancy with respect to the full result at large values. The muon observable z_μ behaves identically to the electron one, z_e.

In conclusion, both the loose minimum di-jet invariant mass cut and the inclusion of QCD radiative correction make the s-channel contributions less suppressed than at LO, making their inclusion mandatory, in order to provide trustworthy predictions at NLO accuracy. Nevertheless, interferences and non-factorizable QCD corrections should be included to reduce the discrepancies down to about 1%, mainly in inclusive anal-

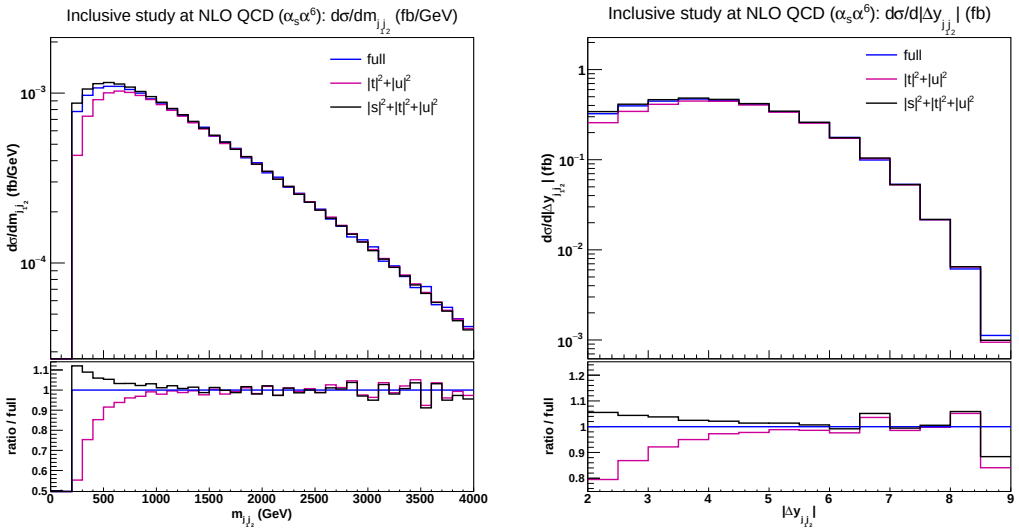

Fig. 6: Differential distributions in the di-jet invariant mass (left) and the rapidity-separation of the two tagging jets (right) at NLO QCD *i.e.* at order $\mathcal{O}(\alpha_s\alpha^6)$ for the full computation and two approximations. The upper plots provide the absolute value for each prediction while the lower plots presents all predictions normalised to MoCaNLO+Recola which is one of the full predictions. In addition to the cuts of Sec. 3.3, the VBS cuts take the values: $m_{jj} > 200\,\text{GeV}$ and $|\Delta y_{jj}| > 2$.

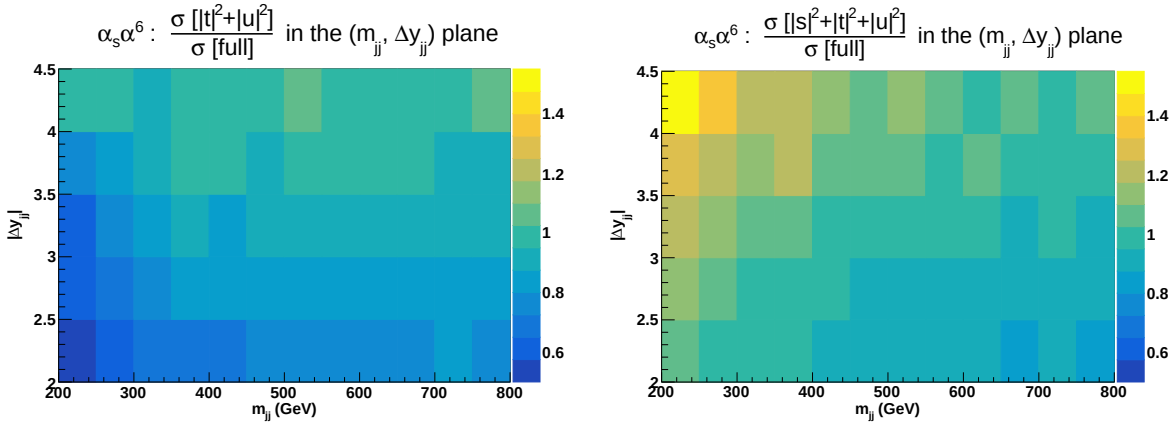

Fig. 7: Ratio of cross sections per bin in the plan $(m_{jj}, |\Delta y_{jj}|)$ at NLO QCD *i.e.* at order $\mathcal{O}(\alpha_s\alpha^6)$ for the VBS approximation over the full computation. Ratio of approximated squared amplitudes over the full matrix element. The approximated squared amplitudes are computed as $|\mathcal{A}|^2 \sim |t|^2 + |u|^2$ (left) and $|\mathcal{A}|^2 \sim |s|^2 + |t|^2 + |u|^2$ (right) In addition to the cuts of Sec. 3.3, the VBS cuts take the values: $m_{jj} > 200\,\text{GeV}$ and $|\Delta y_{jj}| > 2$.

yses. Instead, the VBS approximation at NLO provides a good approximation of full calculations in the kinematic region where VBS contributions are dominant ($M_{jj} \gtrsim 600\,\text{GeV}$, $|\Delta y_{jj}| \gtrsim 3$), for both total cross section and differential distributions.

5.2 Comparison in the fiducial region

In Tab. 5, the cross sections of the various tools at NLO-QCD accuracy are presented. The order considered is again the order $\mathcal{O}(\alpha_s\alpha^6)$ and the fiducial volume is the one described in Sec. 3.3. In contrast with Tab. 3, the NLO predictions differ visibly according to the approximations used.

The first observation is that the predictions featuring two versions of the VBS approximation (Bonsay and the Powheg-Box) are relatively close ([MP: Final number to be added]) [8]. This means that the double-pole approximation on the two W bosons used in Bonsay constitutes a good approximation of the

[8] The VBFNLO-predictions omitting s-channel contributions amounts to 1.3703(1) fb.

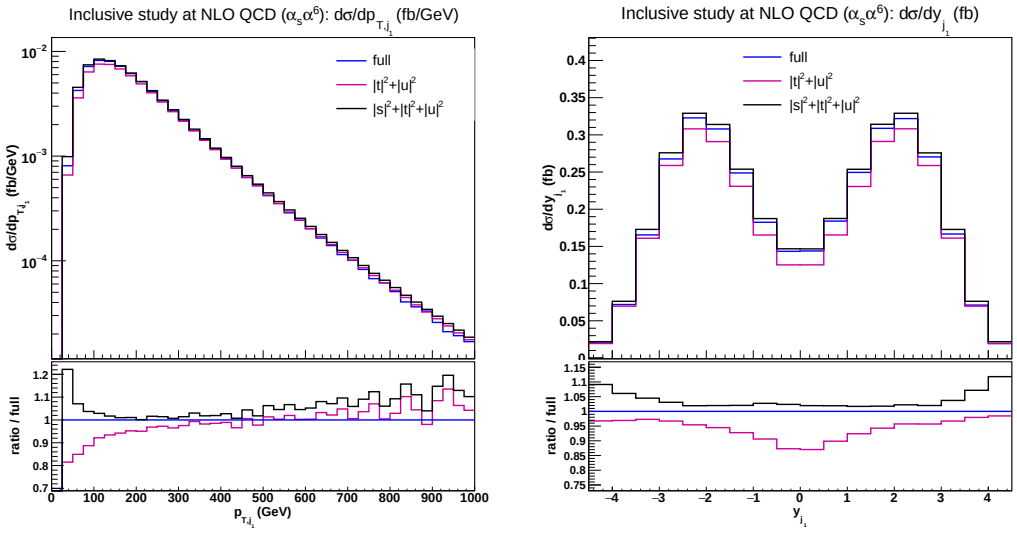

Fig. 8: Differential distributions in the transverse momentum (left) and rapidity of the hardest tagging jet (right) at NLO QCD *i.e.* at order $\mathcal{O}(\alpha_s\alpha^6)$ for the full computation and two approximations. The upper plots provide the absolute value for each prediction while the lower plots presents all predictions normalised to MoCaNLO+Recola which is one of the full predictions. In addition to the cuts of Sec. 3.3, the VBS cuts take the values: $m_{jj} > 200\,\text{GeV}$ and $|\Delta y_{jj}| > 2$.

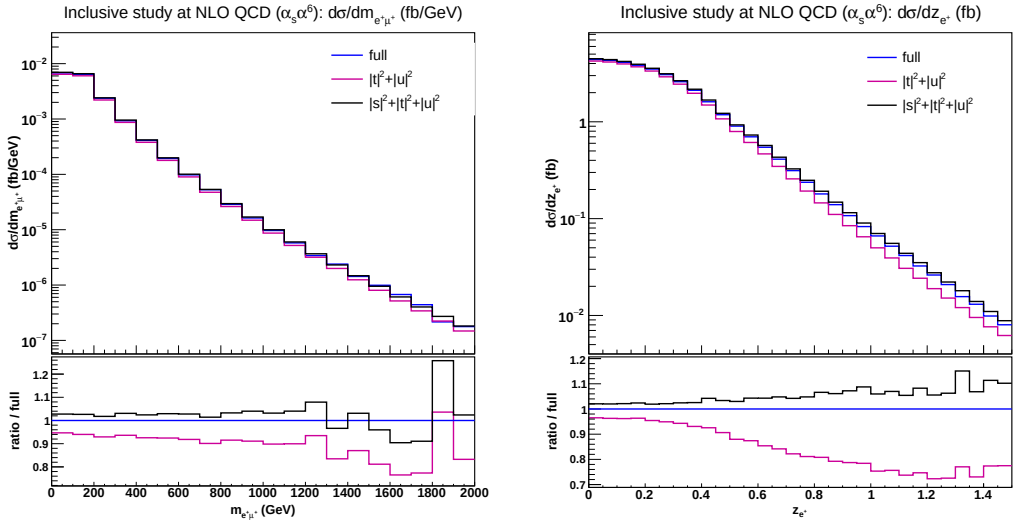

Fig. 9: Differential distributions in the lepton-lepton invariant mass (left) and the electron Zeppenfeld variable (right) at NLO QCD *i.e.* at order $\mathcal{O}(\alpha_s\alpha^6)$ for the full computation and two approximations. The upper plots provide the absolute value for each prediction while the lower plots presents all predictions normalised to MoCaNLO+Recola which is one of the full predictions. In addition to the cuts of Sec. 3.3, the VBS cuts take the values: $m_{jj} > 200\,\text{GeV}$ and $|\Delta y_{jj}| > 2$.

VBS-approximated virtual corrections implemented in the Powheg-Box. Both predictions differ by about 2% with respect to the full computation (MoCaNLO+Recola). The second observation is that the inclusion of s-channel contributions seems to have a significant impact. Indeed, its inclusion (as done in VBFNLO) approximates the full computation by less than a per-cent (0.7%). The main source of the s-channel diagrams thereby consists of real-emission contributions, where one of the two leading jets is formed by one quark, or possibly also both quarks, originating from the W decay, and the second one by the extra radiation emitted from the initial state. In such configurations, the hadronically decaying W boson can become on-shell and hence yield larger

Code	σ[fb]
Bonsay	1.35039 ± 0.00006
MG5_aMC	1.363 ± 0.004
MoCaNLO+Recola	1.378 ± 0.001
Powheg-Box	1.362 ± 0.001
VBFNLO	1.3916 ± 0.0001

Table 5: Cross sections for the LHC process pp $\to \mu^+\nu_\mu e^+\nu_e jj$ at NLO accuracy and order $\mathcal{O}(\alpha_s\alpha^6)$. The uncertainties shown refers to estimated statistical error of the Monte Carlo programs. The predictions are obtained in the fiducial region described in Sec. 3.3.
[MP: Please add or check your respective numbers.]
[MR: My t-/u-channel-only number is 1.3703(1), so something additionally must be going on with Powheg, which we should comment on.] [AK: The number here was wrong. I have updated the table and plots. I am also running some more statistics...]

contributions than at LO, where the invariant mass cut on the two jets forces the boson into the far off-shell region. In Figs. (10-12), several differential distributions are shown. All these predictions are performed at NLO accuracy at the order $\mathcal{O}(\alpha_s\alpha^6)$.

We start with Fig. 10 which displays the invariant mass (left) and the rapidity separation (right) of the two tagging jets. For high invariant mass, all predictions agree rather well. On the other hand, for low invariant mass, the hierarchy present at the level of the cross section is here reproduced. The VBS-approximated predictions (Bonsay and Powheg-Box) are lower than the full calculation (MoCaNLO+Recola). The full calculation is rather well approximated by the hybrid VBS approximation implemented in MadGraph5_aMC@NLO. Finally, VBFNLO which includes as well s-channel contributions provides larger predictions at low invariant mass. For the rapidity difference between the two tagging jets, the hierarchy between the predictions is rather similar. Therefore, depending on the approximation used, it can vary by ±7% and ±4% with respect to the full computation at low invariant mass and low rapidity difference for the tagging jets, respectively

Concerning the transverse momentum (left) and rapidity (right) of the hardest jet shown in Fig. 11, the situation is rather different. While MadGraph5_aMC@NLO is very close to the full prediction for low transverse momentum, it is diverging from it at larger transverse momentum by about 10%. This difference can be attributed to EW Sudakov logarithms that become large in this phase-space region. This is in contrast with the VBS-approximated predictions such as Bonsay, Powheg, and VBFNLO which are lower than the full computation at low transverse momentum and higher for larger transverse momentum. While, the predictions of Bonsay and Powheg are rather close over the whole range, the one of VBFNLO is very different different at low transverse momentum where it is even higher than the full computation. Concerning the rapidity of the hardest jet, VBFNLO is in good agreement with MoCaNLO+Recola in the rapidity range $|y_{j_1}| < 3$. For larger rapidity, the other codes constitute a better description of the full process at order $\mathcal{O}(\alpha_s\alpha^6)$.

The last set of differential distributions is the invariant mass of the two charged lepton (left) and the Zeppenfeld variable for the anti-muon (right). Concerning the comparison of the predictions, both distributions display a rather similar behaviour. Indeed, the hierarchy mentioned previously is here respected and enhanced towards high invariant mass or high Zeppenfeld variable. The predictions of MoCaNLO+Recola and VBFNLO are in rather good agreement for both distributions for the kinematic range displayed here. The other three VBS approximations are close to each other within few per cent.

In the end, the quality of the VBS-approximations amount to tenths of per cent depending on the observables and phase-space range. These differences are larger than at what is observed at LO.

The contributions from s-channel amplitude can be sizeable especially at low invariant mass for the two tagging jet (comparing the predictions of VBFNLO against the ones of Bonsay and Powheg). This can be explained by the fact that s-channel contributions are less suppressed at NLO. In the real, an extra gluon-jet can be radiated from any of the charged particles while the two quarks originating from the W-boson decay can be recombined in a single jet. Therefore, the jet requirements ($m_{jj} > 500\,\text{GeV}$ and $|\Delta y_{jj}| > 2.5$) that were suppressing s-channel contributions at LO are partially lifted with the inclusion of a third jet at NLO. Such an effect has also been observed for top–antitop production in the lepton+jet channel at NLO QCD [74].

At the s-channel contributions are sizeable, their interferences with the t/u-channel can be of similar size in the phase-space region where the former are large. This can be observed by comparing the predictions of VBFNLO against the ones of MadGraph5_aMC@NLO.

Finally, the effect of EW corrections and non-factorisable contributions in the virtual corrections are usually small. But they can be particularly large (about 10%) for large transverse momentum of the hardest jet. These high-energy region of the phase space are where EW Sudakov logarithms become large. Nonetheless these regions are rather suppressed and thus these effects are hardly visible at the level of the cross section.

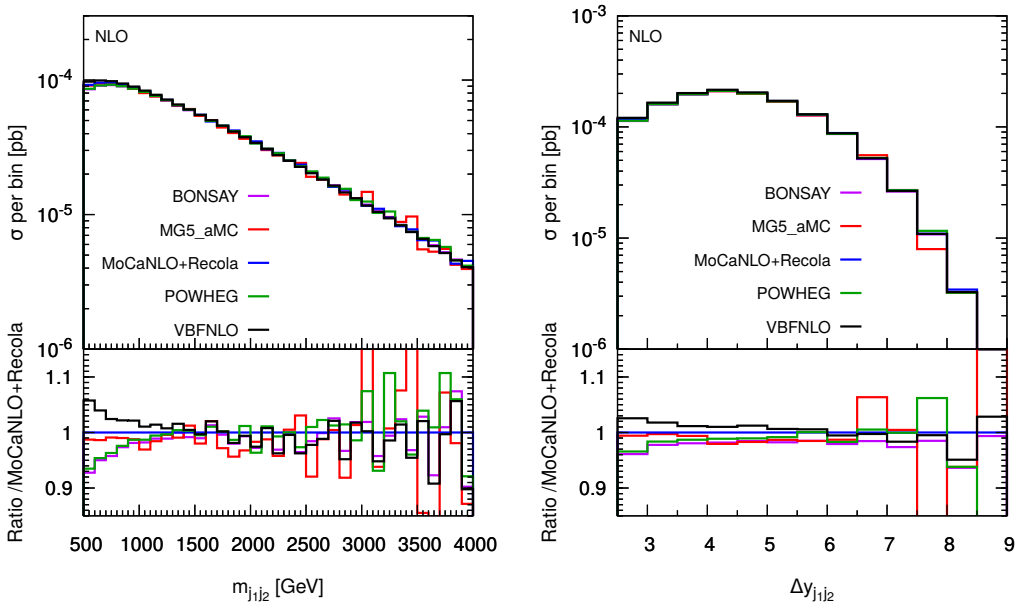

Fig. 10: Differential distributions in the invariant mass (left) and rapidity difference of the two tagging jets (right). The LHC process considered is pp $\to \mu^+\nu_\mu e^+\nu_e jj$ at NLO accuracy and order $\mathcal{O}(\alpha_s\alpha^6)$. The description of the different programs used can be found in Sec. 3.2. The upper plots provide the absolute value for each prediction while the lower plots presents all predictions normalised to MoCaNLO+Recola which is one of the full predictions. The predictions are obtained in the fiducial region described in Sec. 3.3.

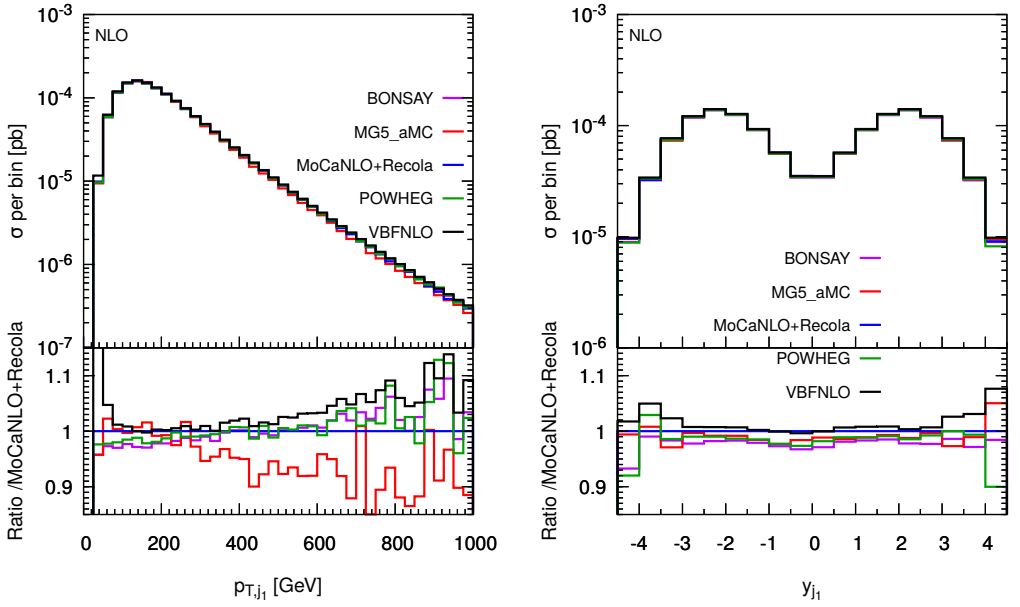

Fig. 11: Differential distributions in the transverse momentum (left) and rapidity of the hardest jet (right). The LHC process considered is pp $\to \mu^+\nu_\mu e^+\nu_e jj$ at NLO accuracy and order $\mathcal{O}(\alpha_s\alpha^6)$. The description of the different programs used can be found in Sec. 3.2. The upper plots provide the absolute value for each prediction while the lower plots presents all predictions normalised to MoCaNLO+Recola which is one of the full predictions. The predictions are obtained in the fiducial region described in Sec. 3.3.

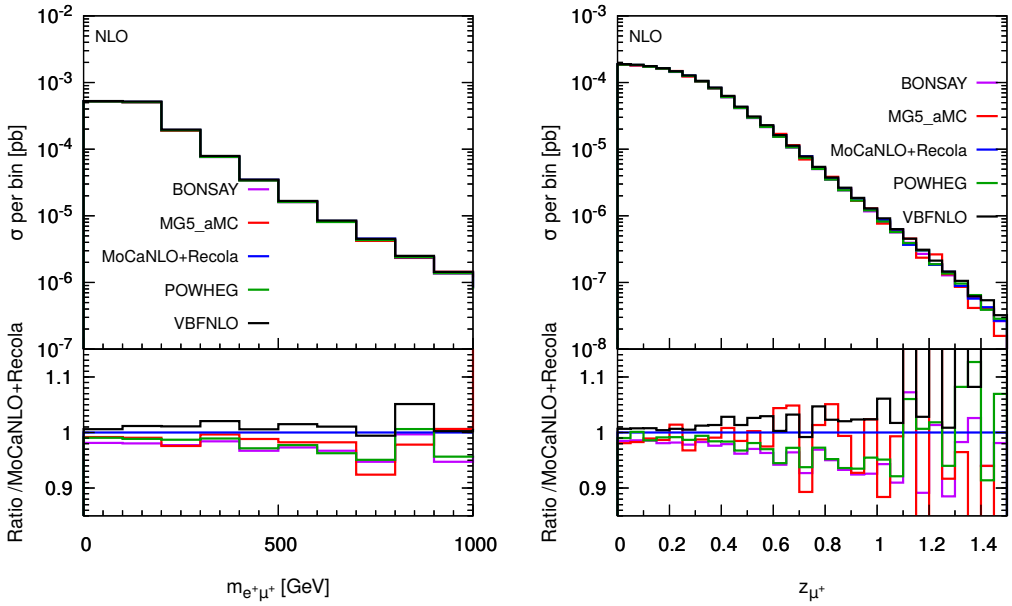

Fig. 12: Differential distributions in the invariant mass of the two charged leptons (left) and Zeppenfeld variable for the muon (right). The LHC process considered is pp $\to \mu^+\nu_\mu e^+\nu_e jj$ at NLO accuracy and order $\mathcal{O}(\alpha_s\alpha^6)$. The description of the different programs used can be found in Sec. 3.2. The upper plots provide the absolute value for each prediction while the lower plots presents all predictions normalised to MoCaNLO+Recola which is one of the full predictions. The predictions are obtained in the fiducial region described in Sec. 3.3.

6 Matching to parton shower

We now discuss how different predictions compare when the matching to parton-shower (PS) is included. For such a comparison we expect larger discrepancy than what we found at fixed-order, as a consequence of the different matching schemes, parton shower employed and of other details of the matching (such as the choice of the parton shower initial scale). Among the codes capable of providing fixed-order results, presented before, MG5_aMC, the Powheg-Box, and VBFNLO can also provide results at (N)LO+PS accuracy. For VBFNLO and the Powheg-Box, we restrict ourselves to showing results only in the VBS approximation, *i.*e. the *s*-channel contributions are neglected here. Besides, also PHANTOM is used for LO+PS results.
MG5_aMC, which employs the MC@NLO [75] matching procedure, will be used together with Pythia8 [76] (version 8.223) and Herwig++ [77, 78] (version 2.7.1). The same parton showers will be employed for the LO results of PHANTOM. For the Powheg-Box, the namesake matching procedure is employed [79, 62], together with Pythia8 (version 8.230). VBFNLO serves as a matrix-element and phase-space provider for the Matchbox module [80] of Herwig7 [81, 82], using an extended version of the BLHA interface [83–85]. The Matchbox module makes it possible to choose between MC@NLO-like and Powheg-like matching. As parton shower, both the default angular-ordered shower as well as the dipole shower can be employed. Whenever Pythia8 is used, the Monash tune [86] is selected.

Results will be presented within the cuts described in Sec. 3.3, applied after shower and hadronisation (this implies that jets are obtained by clustering stable hadrons, and not QCD partons). It follows that at the event-generation level, looser cuts (or even no cuts at all) must be employed in order not to bias the results.

Compared to the fixed order computations, a slightly different set-up has been employed for MG5_aMC in order to simplify the calculation: instead of generating the full pp $\to \mu^+\nu_\mu e^+\nu_e jj$ process, since it is anyway dominated by doubly-resonant contribution, the events are produced for the process with two stable W^+ bosons (pp $\to W^+W^+jj$), and these W^+ bosons are decayed with MadSpin [87] (keeping spin correlations) before the PS. Since MadSpin computes the partial and total decay width of the W bosons at LO accuracy only, while in Section 3.3 the NLO width is employed, a small effect (6%) on the normalisation of distribution is induced. Finally, when the renormalisation and factorisation scales are set, the $\Delta R_{j\ell}$ cut is not imposed during the jet-clustering procedure. But this effect is below a per cent at the level of the fiducial cross sections.

Code	σ[fb]
MG5_aMC+Pythia8	1.352 ± 0.003
MG5_aMC+Herwig++	1.343 ± 0.003
MG5_aMC+Pythia8, $\Gamma_{\rm resc}$	1.275 ± 0.003
MG5_aMC+Herwig++, $\Gamma_{\rm resc}$	1.267 ± 0.003
PHANTOM+Pythia8	1.235 ± 0.001
PHANTOM+Herwig++	1.260 ± 0.001
VBFNLO+Herwig7	1.3001 ± 0.0002

Table 6: Rates at LO-QCD accuracy matched to parton shower within VBS cuts obtained with the different codes used in this comparison, for the pp $\to \mu^+\nu_\mu e^+\nu_e jj$ process. The MG5_aMC results with $\Gamma_{\rm resc}$ are rescaled to account for the effect related to the boson widths computed by MadSpin (see the text for details).

Code	σ[fb]
MG5_aMC+Pythia8	$1.450^{+2\%+2\%}_{-1\%-2\%}$ ± 0.004
MG5_aMC+Herwig++	1.445 ± 0.004
MG5_aMC+Pythia8, $\Gamma_{\rm resc}$	1.368 ± 0.004
MG5_aMC+Herwig++, $\Gamma_{\rm resc}$	1.363 ± 0.004
Powheg-Box	1.3642 ± 0.0004
VBFNLO+Herwig7-Dipole	$1.3389^{+0\%}_{-1\%}$ ± 0.0006
VBFNLO+Herwig7-Default	1.3067 ± 0.0006

Table 7: Rates at NLO-QCD accuracy matched to parton shower within VBS cuts obtained with the different codes used in this comparison, for the pp $\to \mu^+\nu_\mu e^+\nu_e jj$ process. The MG5_aMC results with $\Gamma_{\rm resc}$ are rescaled to account for the effect related to the boson widths computed by MadSpin (see the text for details). For VBFNLO+Herwig7-Dipole, the three-point scale uncertainties are shown, while for MG5_aMC+Pythia8 the two displayed uncertainties are respectively the nine-point scale uncertainty and the PDF one.

We now present the results of predictions matched to parton shower: the total rates within VBS cuts are displayed in Tables 6 and 7, at LO and NLO accuracy respectively. For MG5_aMC, the numbers with $\Gamma_{\rm resc}$ are rescaled to take into account the width effects described in the above paragraph. At NLO accuracy, for MG5_aMC + Pythia8 and VBFNLO-Dipole, we also quote theoretical uncertainties: for the former, we show both PDF and scale uncertainties (a preliminar study on PDF uncertainties in VBS has appeared in Ref. [88]), obtained via exact reweighting [44] by varying independently the renormalization and factorization scale by a factor of two around its central value, Eq. (6) (nine-point variations); for the latter, we show the three-point scale uncertainties, obtained by considering correlated variations of the renormalization and factorization scales. Theory uncertainties should have very little dependence on the tool employed. We observe that, once the width effect is taken into account, total rates from different tools agree within a few per cent, both at LO and NLO. Larger discrepancies, however, will appear for differential observables, which we are going to discuss in the following. Before turning to the differential observables, we point out the smallness of the theory uncertainties due to the scale variations, both when scales are varied independently and when they are varied in a correlated manner, as well as those due to PDF. Concerning differential kinematic distributions, for each observable we will display results in two plots, shown side-by-side. In the plot on the left (right), (N)LO+PS predictions are shown with different colours in the main frame. In the inset, these predictions are compared in both cases with a fixed-order prediction at NLO accuracy (obtained with VBFNLO *i.e.* the VBS approximation with s-channel [BJ: Note that first paragraph of the Sec. says that s-channel contributions are neglected in VBFNLO.] For the differential observables, the MG5_aMC predictions are *not* rescaled to compensate for the width effect mentioned above. As for the table, we show theoretical uncertainties for the NLO+PS samples obtained with VBFNLO and MG5_aMC: again, for the first the band corresponds to three-point variations, while for the second the darker (lighter) band corresponds to nine-point scale variations (plus PDF uncertainties, linearly added).

The first observable we investigate is the exclusive jet multiplicity, shown in Fig. 13. Looking at the LO+PS predictions, one can appreciate that the main effects are driven by the parton shower that is employed (Herwig++/7 or Pythia8), with the clear tendency of producing more radiation for the latter, leading to higher jet multiplicities. Difference among tools that employ the same parton shower are typically smaller, and can be traced back to different values of the initial scale of the parton shower. The main effect of NLO corrections for this (rather inclusive) observable is to stabilise the predictions for the two-jet bin, where discrepancies among tools are reduced to about 10%. For the three-jet bin, which is described only at LO accuracy, differences among tools remain large: the largest rate is predicted by MG5_aMC, while the smallest rate is predicted by the Powheg-Box, both matched to Pythia8. Despite the fact that the same parton shower is employed, the way emissions are treated is different among the two tools. In particular, for the Powheg-Box, the first emission is generated with an internal Sudakov form factor (the prediction dubbed Powheg-no shower corresponds to stopping after the first emission), while

for MG5_aMC there is an interplay between the real-emission matrix element and the shower emission.

The next observable that we study is the invariant mass of the two tagging jets, shown in Fig. 14. For this observable, both at LO+PS and NLO+PS, the spread of predictions matched with parton shower is rather small ($\lesssim 10\%$, if one compensates for the 6% width effect for MG5_aMC); LO+PS predictions tend to be significantly softer than the fixed NLO one, with an effect of about -30% at the end of the displayed range. At NLO+PS, this effect is much more mitigated, owing to the better description of the first QCD emission which is now driven by the real-emission matrix element.

The rapidity difference between the two tagging jets, shown in Fig. 15, has some similarities to the invariant-mass distribution: at LO+PS all predictions, except for VBFNLO3+Herwig7 where the effect is mitigated, show the tendency to deplete the large-separation region with respect to the fixed-order prediction, in a quantitatively similar way. At NLO+PS, when the extra radiation is described by the real matrix element, such an effect is greatly reduced. A notable exception is the Powheg-Box prediction, which still shows a suppression at large separations: since such a suppression is already there for the Powheg-no shower sample, it is very likely that it is driven by the way the first emission is generated. A minor effect in the same direction is visible in the last two bins of the MG5_aMC+Herwig++ prediction (although with rather large statistical uncertainties).

The transverse momentum of the hardest and second-hardest jets are shown in Figs. 16 and 17, respectively. In general, for both observables, predictions from different tools agree rather well with each other, with a spread at most at the 10% level. At LO+PS, typically the transverse-momentum spectra are softer than the fixed-NLO ones, and this effect is more marked for the second-hardest jet which, as expected, is more sensitive to the description of the extra radiation. Again, this effect is mitigated by NLO corrections. The only feature that may be worth noticing among the NLO+PS predictions is the tendency of the Powheg-Box to suppress the hardest-jet spectrum at low transverse momentum ($p_{\mathrm{T,j_1}} < 100\,\mathrm{GeV}$).
If we consider the rapidity of the second jet, Fig. 18, we observe again rather small differences among tools, with the tendency towards a general stabilisation at NLO+PS. However, some (small) differences in the shape remain at NLO+PS, which are worth to be briefly discussed: predictions obtained with MG5_aMC are very close to the fixed-order prediction; the Powheg-Box displays an enhancement of the central region, and a consequent suppression in the peripheral region, while VBFNLO shows an opposite behaviour. However, the effect is rather small, with the largest departure from the fixed-order prediction being at most 10%.[9]

Finally, focusing on the third jet, we conclude the list of differential observables with showing the Zeppenfeld variable defined in Eq. (12), Fig. 19. This variable is closed related to the third jet rapidity, and small (large) value of z correpsond to central (peripheral) rapidities. In general, for observables which involve the third jet, one can clearly see a degradation of the agreement among the various tools, because of the poorer perturbative description of these observables. The Zeppenfeld variable is a striking example: both at LO and NLO, the tendency of Pythia8 to generate more hard and central radiation, corresponding to low values of z, is clearly visible. Such an effect, which is related to the way Pythia8 deals with the recoil of the radiation in VBF(VBS)-type processes, can be mitigated by setting `SpaceShower:dipoleRecoil = on` in the Pythia8 input file;[10] it is interesting to notice that the effect survives beyond the first emission, as it can be observed by comparing Powheg-no shower with Powheg+Pythia8. A similar behaviour of Pythia8 has also been observed in the study of EW production of a Z boson in association with two jets (see the recent CMS measurement, Ref. [89] Figure 12), where the experimental data seem to prefer the description by Herwig++. The central enhancement is a bit mitigated if NLO+PS tools are used (compare LO+PS and NLO+PS from MG5_aMC+Pythia8 with the fixed-NLO prediction), however even at NLO+PS the central region ($z_{j_3} < 0.5$) is cursed by huge differences between tools. Large differences, reaching a factor 2, persist also away from the central region.

In conclusion, the comparison of tools including matching with parton-shower clearly shows the benefits of the inclusion of NLO corrections: for most observables described effectively at NLO accuracy differences between tools are at (or below) the 10% level. Some exceptions exist, *e.g.* the rapidity separation of the two tagging jets, which on the one hand clearly suggest not to rely on a single tool/parton shower, and on the other make it worth to investigate more in details the way

[9] If the setting `SpaceShower:dipoleRecoil = on` (discussed in the following of the article) is used when Pythia8 is employed together with the Powheg-Box, the enhancement at central rapidities and the depletion at small value of transverse momentum are partially compensated.

[10] this requires version ≥ 8.230. Note that such a setting is not compatible with the NLO matching in MG5_aMC (but it is compatible with the Powheg matching). Also, this setting has other effects, though smaller, on the rapidity spectra of the two hardest jets.

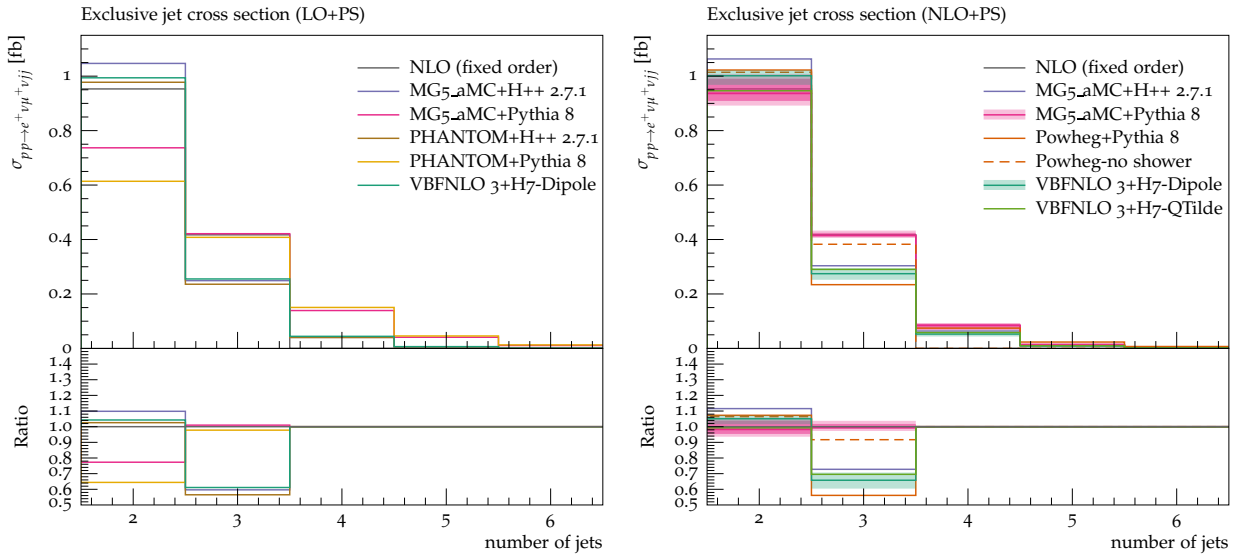

Fig. 13: Exclusive jet multiplicity from predictions matched to parton shower, at LO (left) or NLO (right) accuracy, compared with the fixed-NLO result computed with VBFNLO. At NLO+PS accuracy, for VBFNLO+Herwig7-Dipole, the three-point scale uncertainties are shown, while for MG5_aMC+Pythia8 the darker and lighter bands correspond respectively to the nine-point scale uncertainty and the scale and PDF uncertainties combined linearly.

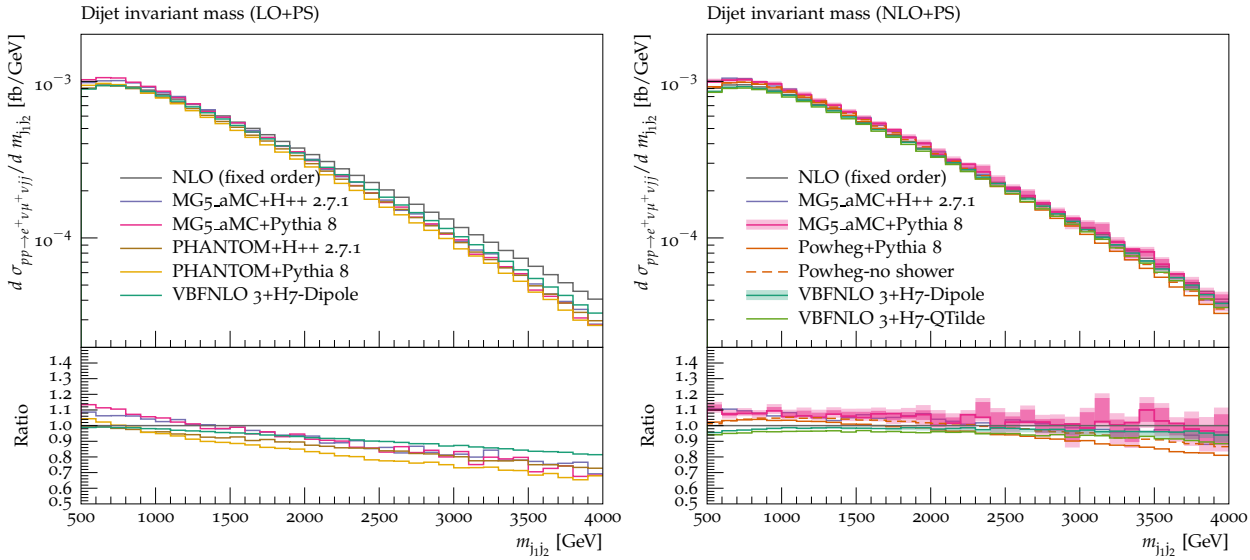

Fig. 14: Same as in Fig. 13, for the invariant mass of the two tagging jets.

QCD radiation is generated, e.g. when fully-differential computations at NNLO will become available (for VBF Higgs production, see Refs. [90, 91]). It is a remarkable fact that, even for those observables that display small discrepancies, the theoretical uncertainty obtained via scale variations systematically underestimates the spread of predictions. Again, this stresses the need to employ at least two different tools in order to have a conservative estimate of theoretical uncertainties. Finally, the size of discrepancies for observables that are described at a lower perturbative accuracy, notably those related to the third jet, suggest that experimental analyses should rely as little as possible on those observables and, in any case, use conservative estimate of the theory uncertainties. On the one hand, in order to improve the description of these observables, a simulation of VBS+j at NLO accuracy, currently unavailable but within the reach of modern automated tools, is certainly desirable;

on the other hand, measurements of processes with similar color flow (EW production of a single vector boson plus jets, VBF, ...) can certainly help in order to discriminate which tools perform better in the comparison with data [92, 89].

7 Conclusion

In the present article, a detailed study of the process $pp \to \mu^+\nu_\mu e^+\nu_e jj + X$ at the LHC has been presented, mainly focused on the electroweak production mechanism which involves the scattering fo massive vector bosons. Until very recently, when the complete calculation became available for the NLO QCD corrections ($\mathcal{O}(\alpha_s\alpha^6)$), the so-called VBS approximation was the standard for this kind of simulations. For this reason, various theoretical predictions have been compared to the full computation, both in a typical VBS fiducial region and also in more inclusive phase-space. We have precisely quantified the differences that arise for several physical observables, in particular for the di-jet invariant mass and the rapidity-separation of the leading two jets. This is the first time that such an in-depth study is performed. Besides the study of fixed-order predictions, we have also investigated the impact of parton-shower. To that end, several LO and NLO event generators which give the possibility to perform matching to parton showers have been employed, and various observables have been thoroughly compared. While in general observables which are described at NLO accuracy show reasonable agreement among the tools, larger differences can appear for those observables described at a lower accuracy, such as those that involve the third jet. These differences appear in the central region where for VBS, and are the largest for those simulations which employ Pythia8. The effect has been understood, and it can be somehow mitigated by changed the recoil scheme of the parton shower. These findings makes it worth to further investigate these issues not only in the theoretical community, but also by experimental collaborations, for example by measuring related observables for similar processes.

The last part of our work is devoted to remarks and recommendations concerning the usage of theoretical predictions by experimental collaborators.

- As found in Ref. [18], the NLO EW corrections of order $\mathcal{O}(\alpha^7)$ are the dominant NLO contribution to the process $pp \to \mu^+\nu_\mu e^+\nu_e jj + X$. It is thus highly desirable that they are combined with NLO-QCD predictions matched with parton shower, or at least that they accounted for by experimental analyses. Since, as shown in [18], these large EW corrections originate from the Sudakov logarithms which factorise, we recommend to combine them with QCD corrections in a multiplicative way. The estimate of missing higher-order EW corrections can be done, in a first approximation, by considering $\pm\delta^2_{\text{NLOEW}}$, while the missing higher-order mixed QCD-EW corrections can be estimated by taking the difference between the multiplicative and additive prescription. For more detailed studies of the combination of QCD and EW higher-order corrections, see e.g., Ref. [93] in the context of top-pair production, or Ref. [94] for SM backgrounds for dark matter searches at the LHC.
- For the typical fiducial region used by experimental collaborations for their measurements, the agreement between the approximations and the full calculation is certainly satisfactory given the current experimental precision, as well as the one foreseen for the near future [MZ: references, etc] . Nonetheless, care has to be taken when using such approximations, in particular if more inclusive phase-space cuts are used.
- In addition to the standard interpretation of EW signal versus QCD background, combined measurements should also be presented as they are better defined theoretically. In fact, while at at LO the interference term can be included in the background component, at NLO the separation of EW and QCD component become more blurred, as, e.g., as at the order $\mathcal{O}(\alpha_s\alpha^6)$ both types of amplitudes mix. Therefore, a combined measurement including the EW, QCD, and interference contributions is desirable. [MZ: the following has to be clarified. one way would be to suggest to use phase-space cuts to enhance/suppress configurations where EW/QCD are the dominant contributions] Note that with such a measurement, an interpretation in terms of EW component is still possible. This would amount to replace the subtraction of the QCD component based on Monte Carlo predictions by an actual measurement. [MP: I am aware that this might be the most touchy point. Therefore we should probably discuss it all together to ensure that we all agree on a definite statement.]
- Since the inclusion of NLO QCD corrections gives a better control of extra QCD radiations and reduces the ambiguites related to the matching details and/or the parton-shower employed, we encourage the use of NLO-accurate event generators in experimental analyses.
- The present study has focused on the orders $\mathcal{O}(\alpha^6)$ at LO and $\mathcal{O}(\alpha_s\alpha^6)$ at NLO. NLO computations

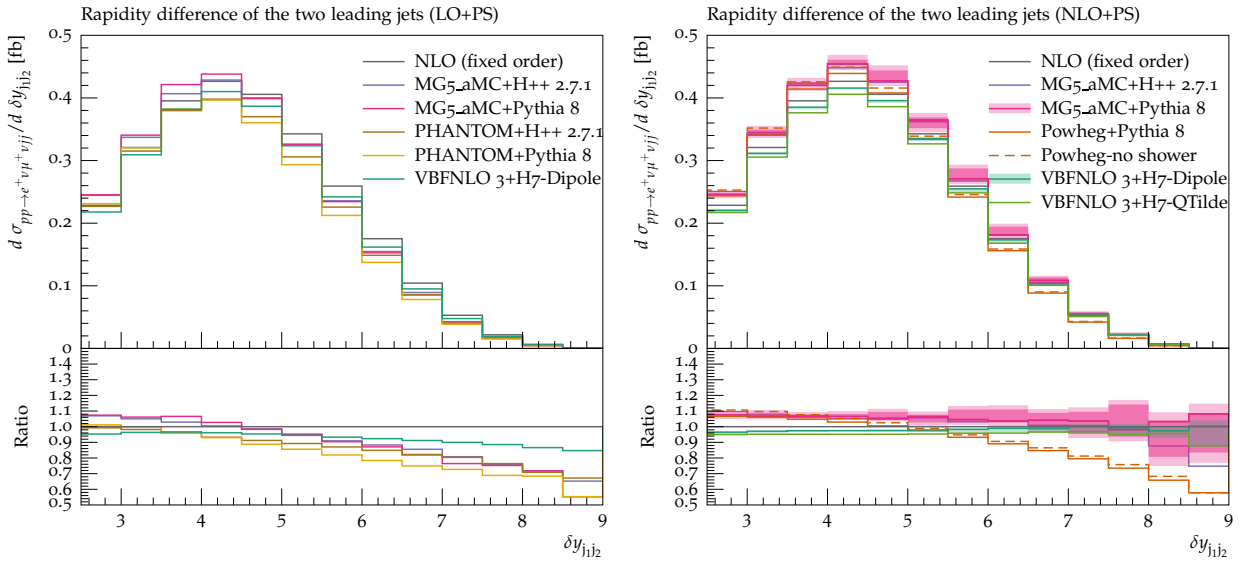

Fig. 15: Same as in Fig. 13, for the rapidity separation of the two tagging jets.

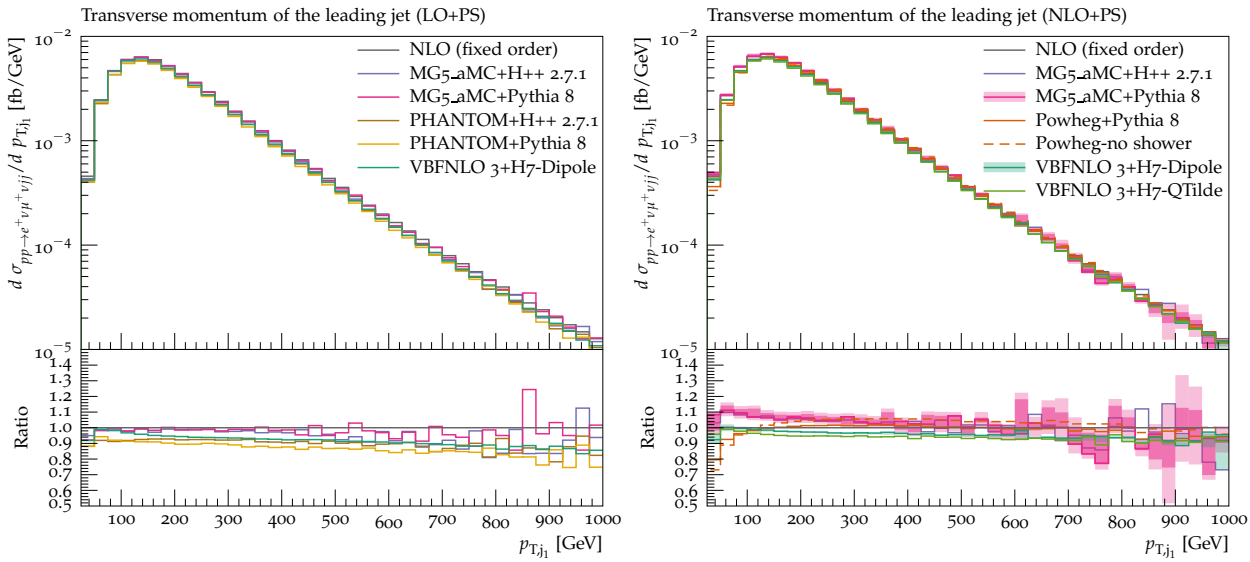

Fig. 16: Same as in Fig. 13, for the transverse momentum of the hardest jet.

and publicly-available tools also exist for the QCD-induced process [12–16, 18, 28].

– For practical reasons, we have focused on the W^+W^+ signature. Nonetheless, the observed features (e.g. validity of the VBS approximation or comparison of theoretical predictions matched to parton shower) should be qualitatively similar for other VBS signatures with massive gauge bosons. For these other signatures, similar quantitative studies should be performed.

Acknowledgements

The authors thank ...
the PYTHIA8 authors, in particular Stefan Prestel, Torbjorn Sjostrand and Peter Skands for discussions and clarifications about the third-jet rapidity spectrum.

The authors would like to acknowledge the contribution of the COST Action CA16108 which initiated this work. Moreover, this work was supported by several STSM Grants from the COST Action CA16108. Many authors acknowledge hospitality from Nikhef, where part of this work has been performed.

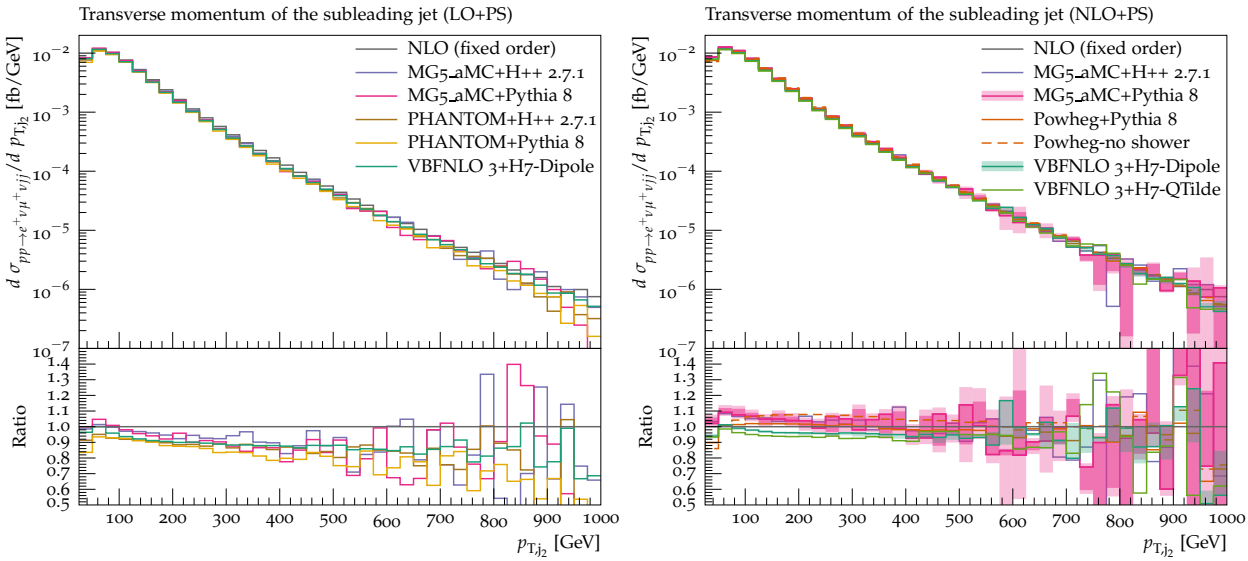

Fig. 17: Same as in Fig. 13, for the transverse momentum of the second-hardest jet.

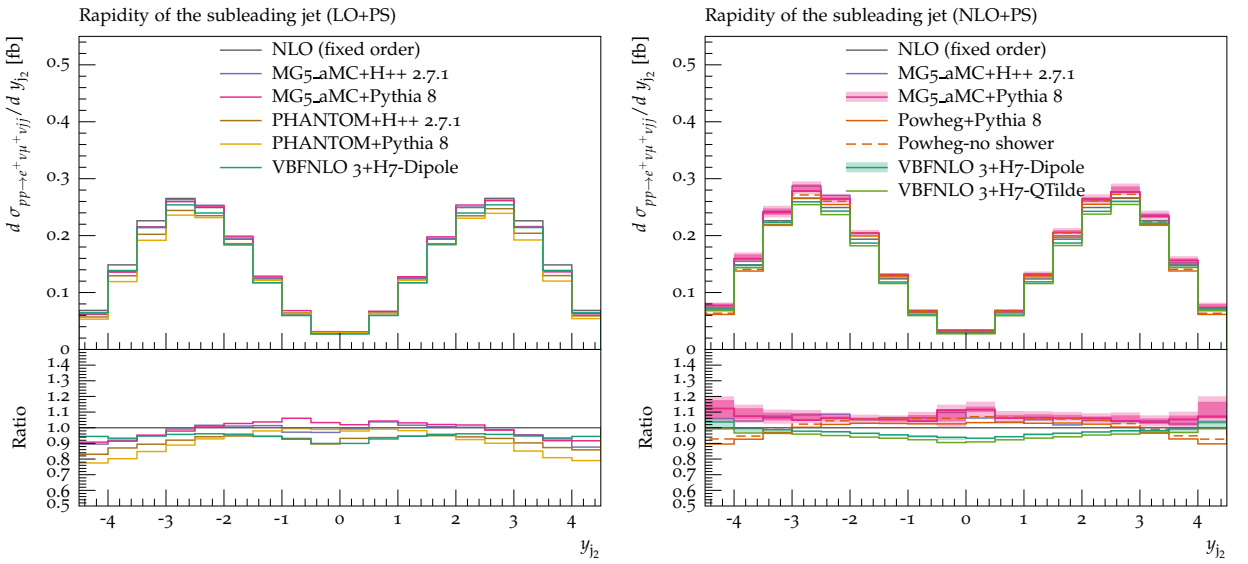

Fig. 18: Same as in Fig. 13, for the rapidity of the second-hardest jet.

BB, AD, and MP acknowledge financial support by the German Federal Ministry for Education and Research (BMBF) under contract no. 05H15WWCA1 and the German Science Foundation (DFG) under reference number DE 623/6-1. AK acknowledges financial support by the Swiss National Science Foundation (SNF) under contract 200020-175595. MR acknowledges funding from the European Union's Horizon 2020 research and innovation programme as part of the Marie Sklodowska-Curie Innovative Training Network MCnetITN3 (grant agreement no. 722104). CS acknowledges support by the state of Baden-Württemberg through bwHPC and the German Research Foundation (DFG) through grant no INST 39/963-1 FUGG and grant DI 784/3. HSS is supported by the ILP Labex (ANR-11-IDEX-0004-02, ANR-10-LABX-63). MZ is supported by the Netherlands National Organisation for Scientific Research (NWO). The work of BJ was supported in part by the Institutional Strategy of the University of Tübingen (DFG, ZUK 63) and in part by the BMBF under contract number 05H2015.

References

1. **ATLAS** Collaboration, G. Aad *et al.*, *Evidence for Electroweak Production of $W^{\pm}W^{\pm}jj$ in pp*

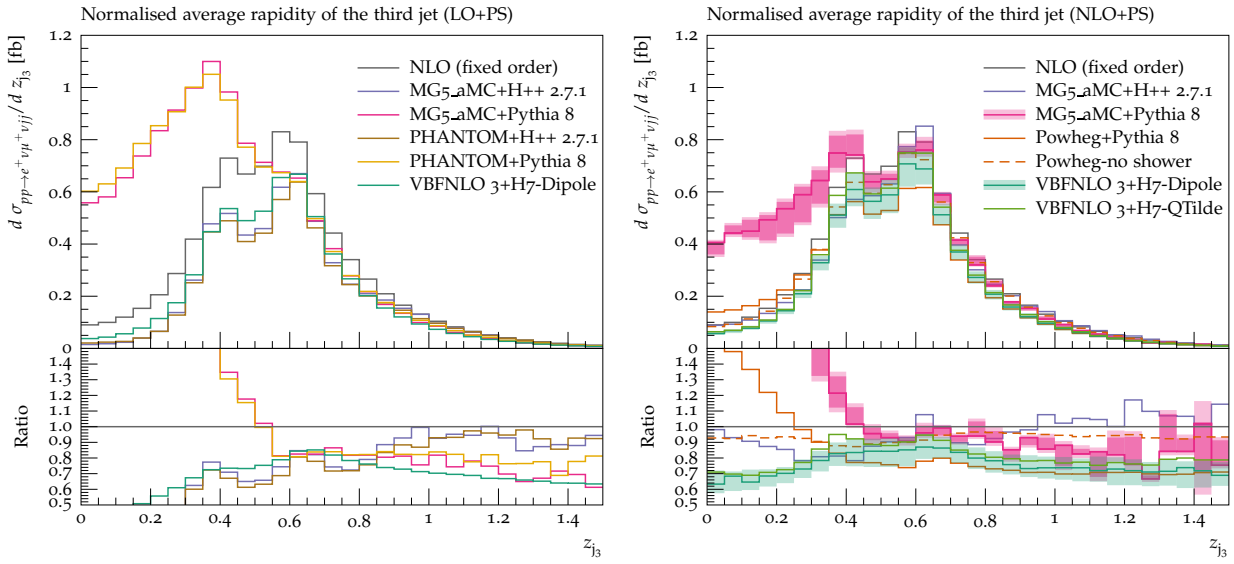

Fig. 19: Same as in Fig. 13, for the z variable of the third-hardest jet.

Collisions at $\sqrt{s} = 8$ TeV with the ATLAS Detector. Phys. Rev. Lett. **113** (2014) no. 14, 141803, arXiv:1405.6241 [hep-ex].

2. **CMS** Collaboration, V. Khachatryan *et al.*, *Study of vector boson scattering and search for new physics in events with two same-sign leptons and two jets*. Phys. Rev. Lett. **114** (2015) no. 5, 051801, arXiv:1410.6315 [hep-ex].
3. **CMS** Collaboration, A. M. Sirunyan *et al.*, *Observation of electroweak production of same-sign W boson pairs in the two jet and two same-sign lepton final state in proton-proton collisions at $\sqrt{s} = 13$ TeV*. arXiv:1709.05822 [hep-ex].
4. **ATLAS** Collaboration, M. Aaboud *et al.*, *Measurement of $W^{\pm}W^{\pm}$ vector-boson scattering and limits on anomalous quartic gauge couplings with the ATLAS detector*. Phys. Rev. **D96** (2017) 012007, arXiv:1611.02428 [hep-ex].
5. **CMS** Collaboration, C. Collaboration, *Prospects for the study of vector boson scattering in same sign WW and WZ interactions at the HL-LHC with the upgraded CMS detector*.
6. B. Jager, C. Oleari, and D. Zeppenfeld, *Next-to-leading order QCD corrections to W+W- production via vector-boson fusion*. JHEP **07** (2006) 015, arXiv:hep-ph/0603177 [hep-ph].
7. B. Jager, C. Oleari, and D. Zeppenfeld, *Next-to-leading order QCD corrections to Z boson pair production via vector-boson fusion*. Phys. Rev. **D73** (2006) 113006, arXiv:hep-ph/0604200 [hep-ph].
8. G. Bozzi, B. Jager, C. Oleari, and D. Zeppenfeld, *Next-to-leading order QCD corrections to W+ Z and W- Z production via vector-boson fusion*. Phys. Rev. **D75** (2007) 073004, arXiv:hep-ph/0701105 [hep-ph].
9. B. Jäger, C. Oleari, and D. Zeppenfeld, *Next-to-leading order QCD corrections to W^+W^+jj and W^-W^-jj production via weak-boson fusion*. Phys. Rev. **D80** (2009) 034022, arXiv:0907.0580 [hep-ph].
10. B. Jäger and G. Zanderighi, *NLO corrections to electroweak and QCD production of W^+W^+ plus two jets in the POWHEGBOX*. JHEP **11** (2011) 055, arXiv:1108.0864 [hep-ph].
11. A. Denner, L. Hošeková, and S. Kallweit, *NLO QCD corrections to W^+W^+jj production in vector-boson fusion at the LHC*. Phys. Rev. **D86** (2012) 114014, arXiv:1209.2389 [hep-ph].
12. M. Rauch, *Vector-Boson Fusion and Vector-Boson Scattering*. arXiv:1610.08420 [hep-ph].
13. T. Melia, K. Melnikov, R. Röntsch, and G. Zanderighi, *Next-to-leading order QCD predictions for W^+W^+jj production at the LHC*. JHEP **12** (2010) 053, arXiv:1007.5313 [hep-ph].
14. T. Melia, P. Nason, R. Röntsch, and G. Zanderighi, *W^+W^+ plus dijet production in the POWHEGBOX*. Eur. Phys. J. **C71** (2011) 1670, arXiv:1102.4846 [hep-ph].
15. F. Campanario, M. Kerner, L. D. Ninh, and D. Zeppenfeld, *Next-to-leading order QCD corrections to W^+W^+ and W^-W^- production in association with two jets*. Phys. Rev. **D89** (2014)

no. 5, 054009, arXiv:1311.6738 [hep-ph].
16. J. Baglio *et al.*, *Release Note - VBFNLO 2.7.0.* arXiv:1404.3940 [hep-ph].
17. C. Oleari and D. Zeppenfeld, *QCD corrections to electroweak nu(l) j j and l+ l- j j production.* Phys. Rev. **D69** (2004) 093004, arXiv:hep-ph/0310156 [hep-ph].
18. B. Biedermann, A. Denner, and M. Pellen, *Complete NLO corrections to W^+W^+ scattering and its irreducible background at the LHC.* JHEP **10** (2017) 124, arXiv:1708.00268 [hep-ph].
19. C. F. Anders *et al.*, "VBSCan Split 2017 Workshop Summary," 2018. arXiv:1801.04203 [hep-ph].
20. I. Kuss and H. Spiesberger, *Luminosities for vector boson - vector boson scattering at high-energy colliders.* Phys. Rev. **D53** (1996) 6078–6093, arXiv:hep-ph/9507204 [hep-ph].
21. E. Accomando, A. Denner, and S. Pozzorini, *Logarithmic electroweak corrections to $e^+e^- \to \nu_e\bar{\nu}_e W^+W^-$.* JHEP **03** (2007) 078, arXiv:hep-ph/0611289 [hep-ph].
22. S. Dawson, *The Effective W Approximation.* Nucl. Phys. **B249** (1985) 42–60.
23. M. J. Duncan, G. L. Kane, and W. W. Repko, *W W Physics at Future Colliders.* Nucl. Phys. **B272** (1986) 517–559.
24. R. N. Cahn and S. Dawson, *Production of Very Massive Higgs Bosons.* Phys. Lett. **136B** (1984) 196. [Erratum: Phys. Lett.138B,464(1984)].
25. S. Dittmaier and M. Roth, *LUSIFER: A LUcid approach to six FERmion production.* Nucl. Phys. **B642** (2002) 307–343, arXiv:hep-ph/0206070 [hep-ph].
26. A. Denner, S. Dittmaier, and L. Hofer, *COLLIER - A fortran-library for one-loop integrals.* PoS **LL2014** (2014) 071, arXiv:1407.0087 [hep-ph].
27. A. Denner, S. Dittmaier, and L. Hofer, COLLIER*: a fortran-based Complex One-Loop LIbrary in Extended Regularizations.* Comput. Phys. Commun. **212** (2017) 220–238, arXiv:1604.06792 [hep-ph].
28. J. Alwall *et al.*, *The automated computation of tree-level and next-to-leading order differential cross sections, and their matching to parton shower simulations.* JHEP **07** (2014) 079, arXiv:1405.0301 [hep-ph].
29. S. Frixione, Z. Kunszt, and A. Signer, *Three jet cross-sections to next-to-leading order.* Nucl. Phys. **B467** (1996) 399–442, arXiv:hep-ph/9512328 [hep-ph].
30. S. Frixione, *A General approach to jet cross-sections in QCD.* Nucl. Phys. **B507** (1997) 295–314, arXiv:hep-ph/9706545 [hep-ph].
31. R. Frederix, S. Frixione, F. Maltoni, and T. Stelzer, *Automation of next-to-leading order computations in QCD: The FKS subtraction.* JHEP **10** (2009) 003, arXiv:0908.4272 [hep-ph].
32. R. Frederix, S. Frixione, A. S. Papanastasiou, S. Prestel, and P. Torrielli, *Off-shell single-top production at NLO matched to parton showers.* JHEP **06** (2016) 027, arXiv:1603.01178 [hep-ph].
33. G. Ossola, C. G. Papadopoulos, and R. Pittau, *Reducing full one-loop amplitudes to scalar integrals at the integrand level.* Nucl. Phys. **B763** (2007) 147–169, arXiv:hep-ph/0609007 [hep-ph].
34. P. Mastrolia, E. Mirabella, and T. Peraro, *Integrand reduction of one-loop scattering amplitudes through Laurent series expansion.* JHEP **06** (2012) 095, arXiv:1203.0291 [hep-ph]. [Erratum: JHEP11,128(2012)].
35. G. Passarino and M. J. G. Veltman, *One-loop corrections for e^+e^- annihilation into $\mu^+\mu^-$ in the Weinberg model.* Nucl. Phys. **B160** (1979) 151–207.
36. A. I. Davydychev, *A Simple formula for reducing Feynman diagrams to scalar integrals.* Phys. Lett. **B263** (1991) 107–111.
37. A. Denner and S. Dittmaier, *Reduction schemes for one-loop tensor integrals.* Nucl. Phys. **B734** (2006) 62–115, hep-ph/0509141.
38. V. Hirschi, R. Frederix, S. Frixione, M. V. Garzelli, F. Maltoni, and R. Pittau, *Automation of one-loop QCD corrections.* JHEP **05** (2011) 044, arXiv:1103.0621 [hep-ph].
39. G. Ossola, C. G. Papadopoulos, and R. Pittau, *CutTools: A Program implementing the OPP reduction method to compute one-loop amplitudes.* JHEP **03** (2008) 042, arXiv:0711.3596 [hep-ph].
40. T. Peraro, *Ninja: Automated Integrand Reduction via Laurent Expansion for One-Loop Amplitudes.* Comput. Phys. Commun. **185** (2014) 2771–2797, arXiv:1403.1229 [hep-ph].
41. V. Hirschi and T. Peraro, *Tensor integrand reduction via Laurent expansion.* JHEP **06** (2016) 060, arXiv:1604.01363 [hep-ph].
42. H.-S. Shao, *Iregi user manual, unpublished.*
43. F. Cascioli, P. Maierhöfer, and S. Pozzorini, *Scattering Amplitudes with Open Loops.* Phys. Rev. Lett. **108** (2012) 111601, arXiv:1111.5206 [hep-ph].

44. R. Frederix *et al.*, *Four-lepton production at hadron colliders: aMC@NLO predictions with theoretical uncertainties*. JHEP **02** (2012) 099, arXiv:1110.4738 [hep-ph].
45. S. Actis *et al.*, *Recursive generation of one-loop amplitudes in the Standard Model*. JHEP **04** (2013) 037, arXiv:1211.6316 [hep-ph].
46. S. Actis *et al.*, *RECOLA: REcursive Computation of One-Loop Amplitudes*. Comput. Phys. Commun. **214** (2017) 140–173, arXiv:1605.01090 [hep-ph].
47. S. Catani and M. H. Seymour, *A general algorithm for calculating jet cross-sections in NLO QCD*. Nucl. Phys. **B485** (1997) 291–419, arXiv:hep-ph/9605323 [hep-ph]. [Erratum: Nucl. Phys. **B510** (1998) 503].
48. S. Dittmaier, *A general approach to photon radiation off fermions*. Nucl. Phys. **B565** (2000) 69–122, arXiv:hep-ph/9904440.
49. A. Denner and R. Feger, *NLO QCD corrections to off-shell top-antitop production with leptonic decays in association with a Higgs boson at the LHC*. JHEP **11** (2015) 209, arXiv:1506.07448 [hep-ph].
50. A. Denner, J.-N. Lang, M. Pellen, and S. Uccirati, *Higgs production in association with off-shell top-antitop pairs at NLO EW and QCD at the LHC*. JHEP **02** (2017) 053, arXiv:1612.07138 [hep-ph].
51. B. Biedermann, A. Denner, and M. Pellen, *Large electroweak corrections to vector-boson scattering at the Large Hadron Collider*. Phys. Rev. Lett. **118** (2017) no. 26, 261801, arXiv:1611.02951 [hep-ph].
52. F. A. Berends, R. Pittau, and R. Kleiss, *All electroweak four fermion processes in electron - positron collisions*. Nucl. Phys. **B424** (1994) 308–342, arXiv:hep-ph/9404313 [hep-ph].
53. A. Denner *et al.*, *Predictions for all processes $e^+e^- \to 4\,fermions + \gamma$*. Nucl. Phys. **B560** (1999) 33–65, arXiv:hep-ph/9904472.
54. A. Ballestrero, A. Belhouari, G. Bevilacqua, V. Kashkan, and E. Maina, *PHANTOM: A Monte Carlo event generator for six parton final states at high energy colliders*. Comput. Phys. Commun. **180** (2009) 401–417, arXiv:0801.3359 [hep-ph].
55. A. Denner *et al.*, *Electroweak corrections to charged-current $e^+e^- \to 4$ fermion processes: Technical details and further results*. Nucl. Phys. **B724** (2005) 247–294, arXiv:hep-ph/0505042.
56. A. Denner and S. Dittmaier, *The Complex-mass scheme for perturbative calculations with unstable particles*. Nucl. Phys. Proc. Suppl. **160** (2006) 22–26, arXiv:hep-ph/0605312 [hep-ph]. [,22(2006)].
57. A. Ballestrero, "PHACT: Helicity amplitudes for present and future colliders," in *High energy physics and quantum field theory. Proceedings, 14th International Workshop, QFTHEP'99, Moscow, Russia, May 27-June 2, 1999*, pp. 303–309. 1999. arXiv:hep-ph/9911318 [hep-ph].
58. A. Ballestrero and E. Maina, *A New method for helicity calculations*. Phys. Lett. **B350** (1995) 225–233, arXiv:hep-ph/9403244 [hep-ph].
59. F. A. Berends, P. H. Daverveldt, and R. Kleiss, *Complete Lowest Order Calculations for Four Lepton Final States in electron-Positron Collisions*. Nucl. Phys. **B253** (1985) 441–463.
60. G. P. Lepage, *A New Algorithm for Adaptive Multidimensional Integration*. J. Comput. Phys. **27** (1978) 192.
61. S. Alioli, P. Nason, C. Oleari, and E. Re, *A general framework for implementing NLO calculations in shower Monte Carlo programs: the POWHEG BOX*. JHEP **06** (2010) 043, arXiv:1002.2581 [hep-ph].
62. S. Frixione, P. Nason, and C. Oleari, *Matching NLO QCD computations with Parton Shower simulations: the POWHEG method*. JHEP **11** (2007) 070, arXiv:0709.2092 [hep-ph].
63. P. Nason and G. Ridolfi, *A Positive-weight next-to-leading-order Monte Carlo for Z pair hadroproduction*. JHEP **08** (2006) 077, arXiv:hep-ph/0606275 [hep-ph].
64. K. Arnold *et al.*, *VBFNLO: A Parton level Monte Carlo for processes with electroweak bosons*. Comput. Phys. Commun. **180** (2009) 1661–1670, arXiv:0811.4559 [hep-ph].
65. K. Arnold *et al.*, *VBFNLO: A Parton Level Monte Carlo for Processes with Electroweak Bosons – Manual for Version 2.5.0*. arXiv:1107.4038 [hep-ph].
66. M. Moretti, T. Ohl, and J. Reuter, *O'Mega: An Optimizing matrix element generator*. arXiv:hep-ph/0102195 [hep-ph].
67. W. Kilian, T. Ohl, and J. Reuter, *WHIZARD: Simulating Multi-Particle Processes at LHC and ILC*. Eur. Phys. J. **C71** (2011) 1742, arXiv:0708.4233 [hep-ph].
68. **NNPDF** Collaboration, R. D. Ball *et al.*, *Parton distributions for the LHC Run II*. JHEP **04** (2015) 040, arXiv:1410.8849 [hep-ph].
69. A. Buckley, J. Ferrando, S. Lloyd, K. Nordström, B. Page, M. Rüfenacht, M. Schönherr, and G. Watt, *LHAPDF6: parton density access in the*

LHC precision era. Eur. Phys. J. **C75** (2015) 132, arXiv:1412.7420 [hep-ph].

70. D. Yu. Bardin, A. Leike, T. Riemann, and M. Sachwitz, *Energy-dependent width effects in e^+e^--annihilation near the Z-boson pole*. Phys. Lett. **B206** (1988) 539–542.
71. A. Denner, S. Dittmaier, M. Roth, and D. Wackeroth, *Electroweak radiative corrections to $e^+e^- \to WW \to 4$ fermions in double-pole approximation: The RACOONWW approach*. Nucl. Phys. **B587** (2000) 67–117, arXiv:hep-ph/0006307 [hep-ph].
72. **CMS** Collaboration, *Observation of electroweak production of same-sign W boson pairs in the two jet and two same-sign lepton final state in proton-proton collisions at 13 TeV*. CMS-PAS-SMP-17-004.
73. M. Cacciari, G. P. Salam, and G. Soyez, *The anti-k_t jet clustering algorithm*. JHEP **04** (2008) 063, arXiv:0802.1189 [hep-ph].
74. A. Denner and M. Pellen, *Off-shell production of top-antitop pairs in the lepton+jets channel at NLO QCD*. JHEP **02** (2018) 013, arXiv:1711.10359 [hep-ph].
75. S. Frixione and B. R. Webber, *Matching NLO QCD computations and parton shower simulations*. JHEP **06** (2002) 029, arXiv:hep-ph/0204244 [hep-ph].
76. T. Sjöstrand, S. Ask, J. R. Christiansen, R. Corke, N. Desai, P. Ilten, S. Mrenna, S. Prestel, C. O. Rasmussen, and P. Z. Skands, *An Introduction to PYTHIA 8.2*. Comput. Phys. Commun. **191** (2015) 159–177, arXiv:1410.3012 [hep-ph].
77. M. Bahr *et al.*, *Herwig++ Physics and Manual*. Eur. Phys. J. **C58** (2008) 639–707, arXiv:0803.0883 [hep-ph].
78. J. Bellm *et al.*, *Herwig++ 2.7 Release Note*. arXiv:1310.6877 [hep-ph].
79. P. Nason, *A New method for combining NLO QCD with shower Monte Carlo algorithms*. JHEP **11** (2004) 040, arXiv:hep-ph/0409146 [hep-ph].
80. S. Platzer and S. Gieseke, *Dipole Showers and Automated NLO Matching in Herwig++*. Eur. Phys. J. **C72** (2012) 2187, arXiv:1109.6256 [hep-ph].
81. J. Bellm *et al.*, *Herwig 7.0/Herwig++ 3.0 release note*. Eur. Phys. J. **C76** (2016) no. 4, 196, arXiv:1512.01178 [hep-ph].
82. J. Bellm *et al.*, *Herwig 7.1 Release Note*. arXiv:1705.06919 [hep-ph].
83. T. Binoth *et al.*, *A Proposal for a standard interface between Monte Carlo tools and one-loop programs*. Comput. Phys. Commun. **181** (2010) 1612–1622, arXiv:1001.1307 [hep-ph]. [,1(2010)].
84. S. Alioli *et al.*, *Update of the Binoth Les Houches Accord for a standard interface between Monte Carlo tools and one-loop programs*. Comput. Phys. Commun. **185** (2014) 560–571, arXiv:1308.3462 [hep-ph].
85. J. R. Andersen *et al.*, *Les Houches 2013: Physics at TeV Colliders: Standard Model Working Group Report*. arXiv:1405.1067 [hep-ph].
86. P. Skands, S. Carrazza, and J. Rojo, *Tuning PYTHIA 8.1: the Monash 2013 Tune*. Eur. Phys. J. **C74** (2014) no. 8, 3024, arXiv:1404.5630 [hep-ph].
87. P. Artoisenet, R. Frederix, O. Mattelaer, and R. Rietkerk, *Automatic spin-entangled decays of heavy resonances in Monte Carlo simulations*. JHEP **03** (2013) 015, arXiv:1212.3460 [hep-ph].
88. S. Dittmaier, P. Maierhöfer, C. Schwan, and F. Siegert, "Vector Boson Scattering (VBS) at the LHC." In: *PoS* RADCOR2017.
89. **CMS** Collaboration, A. M. Sirunyan *et al.*, *Electroweak production of two jets in association with a Z boson in proton-proton collisions at $\sqrt{s} =$ 13 TeV*. arXiv:1712.09814 [hep-ex].
90. M. Cacciari, F. A. Dreyer, A. Karlberg, G. P. Salam, and G. Zanderighi, *Fully differential Vector-Boson-Fusion Higgs production at Next-to-Next-to-Leading Order*. Phys. Rev. Lett. **115** (2015) no. 8, 082002, arXiv:1506.02660 [hep-ph].
91. J. Cruz-Martinez, T. Gehrmann, E. W. N. Glover, and A. Huss, *Second-order QCD effects in Higgs boson production through vector boson fusion*. arXiv:1802.02445 [hep-ph].
92. **ATLAS** Collaboration, M. Aaboud *et al.*, *Measurement of the cross-section for electroweak production of dijets in association with a Z boson in pp collisions at $\sqrt{s} =$ 13 TeV with the ATLAS detector*. Phys. Lett. **B775** (2017) 206–228, arXiv:1709.10264 [hep-ex].
93. M. Czakon, D. Heymes, A. Mitov, D. Pagani, I. Tsinikos, and M. Zaro, *Top-pair production at the LHC through NNLO QCD and NLO EW*. JHEP **10** (2017) 186, arXiv:1705.04105 [hep-ph].
94. J. M. Lindert *et al.*, *Precise predictions for V+ jets dark matter backgrounds*. Eur. Phys. J. **C77** (2017) no. 12, 829, arXiv:1705.04664 [hep-ph].